



FP7-ICT Future Networks  
SPECIFIC TARGETTED RESEARCH PROJECT  
Project Deliverable

<b>PHYDYAS Doc. Number</b>	PHYDYAS_024
<b>Project Number</b>	ICT - 211887
<b>Project Acronym+Title</b>	PHYDYAS - PHYsical layer for DYnamic AccesS and cognitive radio
<b>Deliverable Nature</b>	Report
<b>Deliverable Number</b>	D6.3
<b>Contractual Delivery Date</b>	July 1st, 2010
<b>Actual Delivery Date</b>	October 29th, 2010
<b>Title of Deliverable</b>	Interference management and cross-layer design
<b>Contributing Work Package</b>	WP6
<b>Project starting date; Duration</b>	01/01/2008; 30 months
<b>Dissemination Level</b>	PU
<b>Author(s)</b>	Leonardo Baltar, Qing Bai, Josef Nosssek (TUM-WP6 leader); Nikos Passas (RA-CTI); Carlos Bader (CTTC); Michel Terré (CNAM)

**Abstract:** The final work performed in WP6 on interference management and cross-layer design in uplink is reported. The performance of an uplink OFDM/FBMC multi-cell network is analyzed. Regarding cross-layer design, resource allocation and scheduling methods developed for downlink are extended to uplink and simulation results are provided. The increased robustness of FBMC as compared to CP-OFDM is demonstrated.

# Contents

<b>1</b>	<b>Introduction</b>	<b>3</b>
1.1	Scope . . . . .	3
<b>2</b>	<b>Interference Management</b>	<b>4</b>
2.1	OFDM/FBMC Interference Tables . . . . .	5
2.2	Unsynchronized Multicarrier Transmission over a Selective Frequency Channel	5
2.2.1	CP-OFDM case . . . . .	5
2.2.2	FBMC case . . . . .	9
2.3	Performance analysis of an uplink OFDM/FBMC multi-cell network . . . .	9
2.3.1	System Model . . . . .	9
2.3.2	Simulation . . . . .	13
2.4	Conclusion . . . . .	20
<b>3</b>	<b>Cross-layer design: resource allocation and scheduling methods</b>	<b>21</b>
3.1	Uplink Resource Allocation in CP-OFDM and FBMC Systems . . . . .	21
3.1.1	Introduction . . . . .	21
3.1.2	Uplink resource allocation algorithm . . . . .	22
3.1.3	Effects and compensation of CFO in the uplink . . . . .	26
3.1.4	Simulation results and analysis . . . . .	30
3.1.5	Conclusions . . . . .	31
3.2	Scheduler description and results . . . . .	33
3.2.1	System description . . . . .	33
3.2.2	Scheduler description . . . . .	35
3.3	Cross-Layer scheduling methods . . . . .	40
3.3.1	Cross-layer schemes in the bibliography . . . . .	41
3.3.2	The cross-layer optimization mechanism . . . . .	41
3.3.3	Decision algorithm . . . . .	43
3.3.4	Simulation model and results . . . . .	44
3.4	Simulation results for the joint scheduling and resource allocation approach	47
<b>4</b>	<b>Conclusions</b>	<b>57</b>
	<b>Bibliography</b>	<b>59</b>

# Chapter 1

## Introduction

### 1.1 Scope

Four tasks have been assigned to workpackage 6, namely duplexing techniques, multiple access techniques, interference management and cross-layer optimization. The objective of the WP is to investigate the impact of FBMC in these different topics and perform a comparison in terms of performance and implementation with OFDM. This document is the third deliverable produced by the WP. Duplexing techniques were dealt with in D6.1. Multiple access techniques have been covered in D6.1 and D6.2. Interference management for the downlink has been considered in D6.2. Regarding cross-layer optimization, the topic was started in D6.1 and continued in D6.2. The objective of D6.3 is to complete the task of interference management investigation by considering the uplink and finalize the work on cross-layer optimization. More specifically, in this document

- the approach of intercell interference tables for multicell network is extended to the uplink and fractional frequency reuse is included,
- cross-layer design (resource allocation and scheduling) is extended to include the uplink.

The algorithms which are developed are validated through simulation and comparison with OFDM is performed.

## Chapter 2

# Interference Management

Interference at the radio receiver is a key source of degradation in quality of service of wireless communication systems. Multicarrier based systems do not suffer from interference among multiplexed users within a cell given perfect synchronization. However, when it comes to a multi-cell environment, heavy inter-cell interferences between adjacent cells are induced and they significantly degrade the system performance and especially, cell edge user performance [1, 2]. Moreover, in some cases such as cognitive radio, non cooperative base stations or Ad-hoc networks, it is very difficult to maintain the synchronization. Consequently, it is relevant to evaluate the impact of the asynchronous interference on the system performance.

Several models have been proposed to investigate this problem such as the classical Gaussian approximation (GA) techniques [3],[4] and the power spectral density (PSD) model of the inter-cell interference [5],[6],[7]. In some cases, the interference is correlated because the accumulated interference is no longer a sum of independent random variables. In these cases, the GA model is inaccurate [8]. The PSD doesn't always give accurate results also. For example, when the timing offset does not exceed the cyclic prefix duration the interference comes only from the same frequency but the other frequencies don't contribute in this interference. Unfortunately, in this case the PSD modeling still shows that the other frequencies contribute in the resulting interference. In [9], a new model of inter-cell interference has been proposed. It is based on the computation of the interference power due to a timing offset and evaluated at the output of the receiver filter. Our aim is to assess the accuracy of the utilization of this model with respect to two criteria: the signal to interference plus noise ratio (SINR) and the user capacity. A comparison with similar results, obtained through intensive Monte Carlo simulations, is presented. In this study, we focus on the uplink of an unsynchronized multi-cellular network. We assume a perfect frequency and time synchronization between the user and its own base station. Hence, the interference will only come from users of other cells. Two multi-carrier modulation techniques are considered: the conventional orthogonal frequency division multiplex using the cyclic prefix (CP-OFDM) and the Filter Bank based Multi-Carrier (FBMC) waveform.

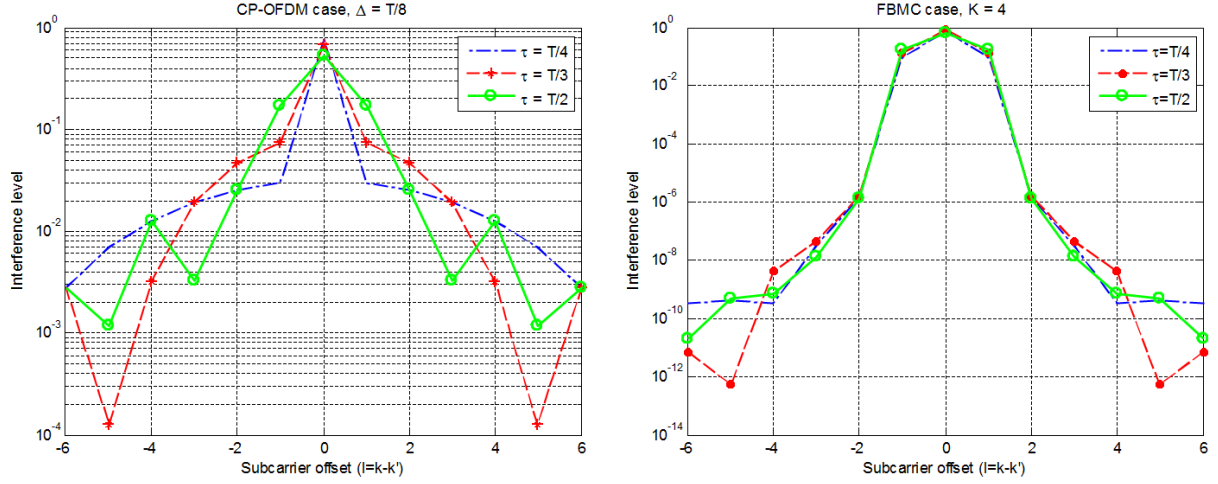


Figure 2.1: The interference level in CP-OFDM ( $\Delta = T/8$ ) and FBMC (PHYDYAS prototype filter with an overlapping factor  $K = 4$ ) for  $\tau = \{T/4, T/3, T/2\}$

## 2.1 OFDM/FBMC Interference Tables

In [10], a new model of inter-cell interference has been proposed for two multicarrier modulation techniques: Orthogonal Frequency Division Multiplexing using the Cyclic prefix (CP-OFDM) and the Filter Bank based Multi-Carrier (FBMC) waveform. It is based on the computation of the interference power at the output of the receiver filter corresponding to a given timing offset. Two tables, modeling the mean interference power, are given for timing offset  $\tau$  uniformly distributed on the OFDM block duration  $T$ . It should be noticed that these tables have been evaluated for a constant unitary channel.

According to Fig. 2.1, we see that the interference in OFDM case is spread over a high number of subchannels. On the other hand, for the FBMC, the interference is more localized and it appears only on the subchannel of interest and the two immediate adjacent ones. We have also shown that the asynchronous interference in a unitary constant channel depends only on the timing offset  $\tau$  and the carrier difference between the victim user and the interferer  $k - k'$ .

The theoretical derivation of these tables has been presented in [10], [9], [11].

## 2.2 Unsynchronized Multicarrier Transmission over a Selective Frequency Channel

### 2.2.1 CP-OFDM case

In a classical OFDM transmission, we choose the cyclic prefix duration ( $\Delta$ ) greater than the maximum delay of the propagation channel ( $\tau_{\max}$ ). In such case, the CP transforms

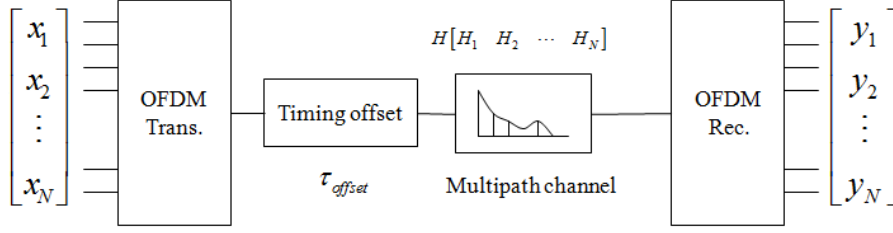


Figure 2.2: Unsynchronized OFDM/FBMC transmission

a linear convolution channel to a cyclic convolution channel. After the FFT operation of the receiver and by neglecting noise, we get:

$$y_k = H_k x_k \quad (2.1)$$

where:  $H_k$  is the channel frequency response and  $k$  is the subcarrier index. However, when the transmitter and the receiver are unsynchronized with a timing offset bigger than the CP duration ( $\tau_{\text{offset}} > \Delta$ ), we can't use the relation (2.1) to compute the received signal. According to [9], the received signal in an unsynchronized transmission with ( $\tau_{\text{offset}} > \Delta$ ) is given by

$$y_{k'}(\tau) = x_k e^{-j\frac{2\pi}{T}k\tau} \int_{\tau}^{T+\Delta} e^{-j\frac{2\pi}{T}lt'} dt' = x_k e^{-j\frac{2\pi}{T}[k\tau+l(\frac{\tau+\Delta}{2})]} \frac{\sin(\pi l(T+\Delta-\tau)/T)}{\pi l} \quad (2.2)$$

where  $k, k'$  denote respectively the subcarriers of the transmission and the reception,  $l = k - k'$  is the offset between them and  $T$  is the OFDM symbol duration. For  $l = 0$ , we have

$$y_k(\tau) = x_k e^{-j\frac{2\pi}{T}k\tau} \frac{T+\Delta-\tau}{T} \quad (2.3)$$

Now, let us consider a multi-path channel with the following impulse response:

$$h(t) = \sum_i h_i(t) \delta\left(t - \frac{n_i}{N}T\right) \quad (2.4)$$

$h_i$  and  $\frac{n_i}{N}T$  are the channel gain and the delay of the  $i$ -th path. Therefore, the received unsynchronized signal over a multi-path channel can be expressed by

$$y_k(\tau) = x_k \sum_i h_i(t) e^{-j\frac{2\pi}{T}k(\tau - \frac{n_i}{N}T)} \frac{T+\Delta-\tau - \frac{n_i}{N}T}{T} \quad (2.5)$$

$$= x_k e^{-j\frac{2\pi}{T}k\tau} \frac{T+\Delta-\tau}{T} \sum_i h_i(t) e^{-j\frac{2\pi}{N}kn_i} + \frac{x_k}{N} e^{-j\frac{2\pi}{T}k\tau} \sum_i n_i h_i(t) e^{-j\frac{2\pi}{N}kn_i} \quad (2.6)$$

$$= x_k e^{-j\frac{2\pi}{T}k\tau} \frac{T+\Delta-\tau}{T} H_k(t) + \underbrace{\frac{x_k}{N} e^{-j\frac{2\pi}{T}k\tau} H'_k}_{\text{error}} \quad (2.7)$$

$$(2.8)$$

where  $H'_k$  is the FFT of the following modified channel impulse response

$$h'(t) = \sum_i n_i h_i(t) \delta\left(t - \frac{n_i}{N}T\right) \quad (2.9)$$

The first term in (2.7) can be computed using the instantaneous interference table and the channel gain at the frequency index  $k$ .

So, we can estimate the received power in unsynchronized transmission over a selective frequency channel by multiplying the transmitted power by the channel gain and the corresponding coefficient of the interference power table.

$$P'_{\text{rec-est}}(t) = P_{\text{tran}} I_{|k-k'|} |H_{k'}|^2, \quad (2.10)$$

where  $I_{|k-k'|}$  is the coefficient of the interference table in [10]. In order to assess the accuracy of this estimation, we compare the estimated power using the interference table to the power calculated via Monte-Carlo simulation. We have considered two multipath channel models (the Pedestrian-A model and the TU50 model-A) with the following parameters

Parameter	Value
Pedestrian fading delays	[0 110 190 410] ns
Pedestrian fading powers	[0 -9.7 -19.2 -22.8] dB
TU 50 fading delays	[0 0.217 0.512 0.514 0.517 0.674 0.882 1.230 1.287 1.311 1.349 1.533 1.535 1.622 1.818 1.836 1.884 1.943 2.048 2.140] $\mu$ s
TU 50 fading powers	[-5.7 -7.6 -10.1 -10.2 -10.2 -11.5 -13.4 -16.3 -16.9 -17.1 -17.4 -19.0 -19.0 -19.8 -21.5 -21.6 -22.1 -22.6 -23.5 -24.3] dB

Table 2.1: Channel parameters used in simulations

Other simulation parameters involved within this study are summarized in Table 2.2 hereafter.

Parameter	Value	Unit
Total bandwidth $B$	10	MHz
Bandwidth per subcarrier	9.5	kHz
Center frequency	2.5	GHz
Number of subcarriers	1024	-
CP duration $\Delta$	12.8 ( $T/8$ )	$\mu$ s
SNR	20	dB

Table 2.2: Statistical simulation parameters

Figure 2.3 shows the power coming from an unsynchronized transmitter with a given timing offset ( $\tau_{\text{offset}}$ ) calculated by the Table estimation and the Monte-Carlo method (over 1000 realizations) for different channel realizations. The channel frequency response is also depicted for each situation. It should be noticed that we assume that the propagation channels are stationary over the whole data frame.

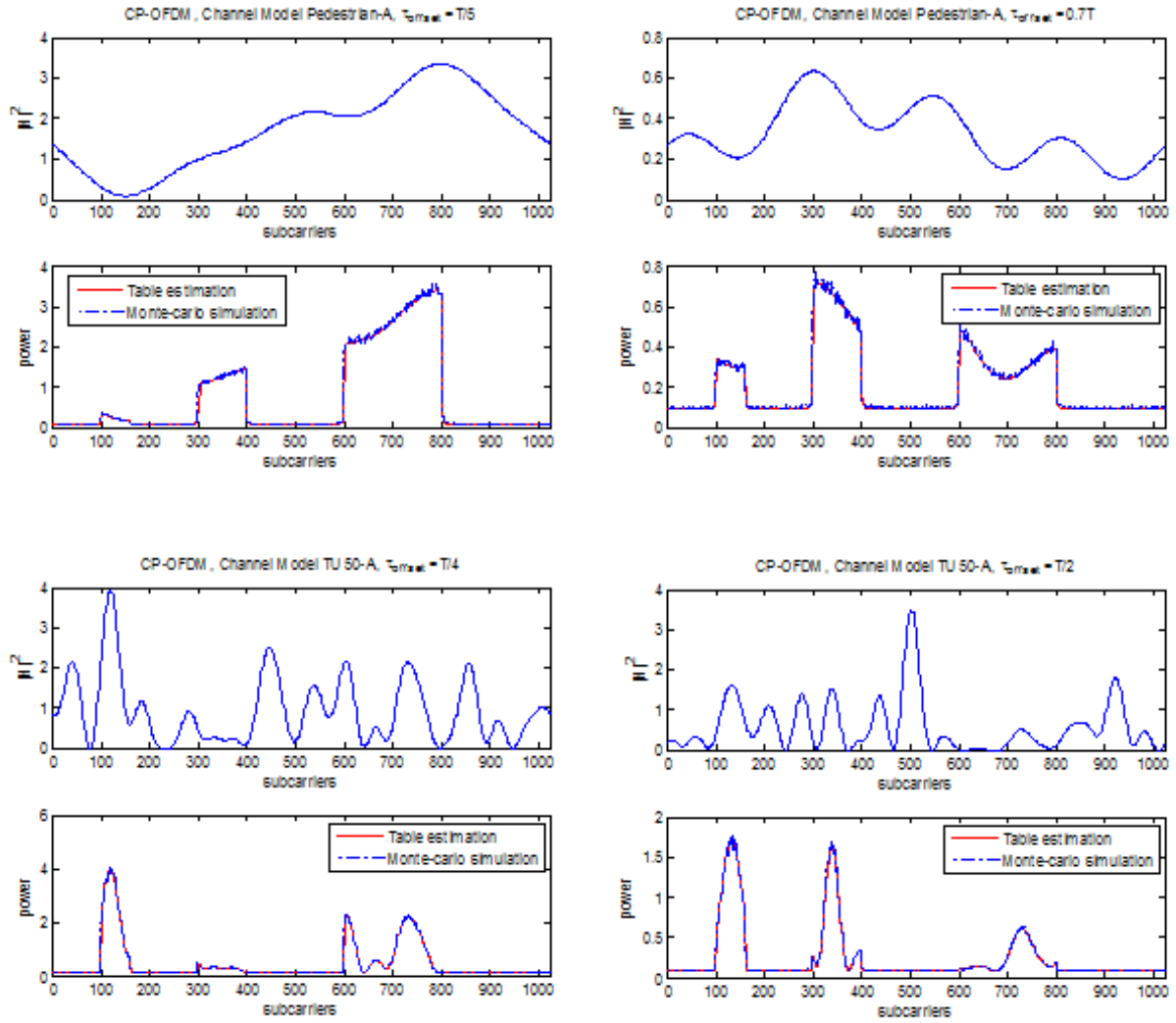


Figure 2.3: Table estimation and the Monte-Carlo comparison, OFDM case



Comparing the Monte-Carlo method (dashed curve) to the Table estimation method (solid curve), we see clearly, that the Table estimation gives an accurate estimation of the power coming from an unsynchronized transmitter over a selective frequency channel. This result is valid for a weak and a strong frequency selective channel (resp. Pedestrian-A and TU 50 models).

### 2.2.2 FBMC case

For the FBMC case, the asynchronous transmitted signal is given by

$$s(t) = [a[n]g(t - nT - \tau) + jb[n]g(t - nT - \tau - T/2)]e^{j(\frac{2\pi}{T}(t-\tau)+\frac{\pi}{2})k} \quad (2.11)$$

$g(t)$  is the real-valued symmetric pulse response of the prototype filter and denotes the timing offset between the transmitter and the receiver. For a unitary channel ( $h(t) = 1$ ), the  $k'$ -th output of the receiver can be expressed [9]

$$\begin{aligned} y_{k'}(\tau) &= (s(t)e^{-j(\frac{2\pi}{T}t+\frac{\pi}{2})k'}) * f(t) \\ &= e^{-j\frac{2\pi}{T}k\tau} \left\{ a[l] \int_{-\infty}^{\infty} g(t - lT - \tau - \alpha) f(\alpha) e^{j(\frac{2\pi}{T}(t-\alpha)+\frac{\pi}{2})(k-k')} d\alpha \right. \\ &\quad \left. + jb[l] \int_{-\infty}^{\infty} g(t - (l + \frac{1}{2})T - \tau - \alpha) f(\alpha) e^{j(\frac{2\pi}{T}(t-\alpha)+\frac{\pi}{2})(k-k')} d\alpha \right\} \end{aligned} \quad (2.12)$$

$f(t)$  is the pulse response of the receiver filter. However, for a multi-path propagation channel with the impulse response defined in (4), the received signal is given by

$$y_{k'}(\tau) = \left[ \sum_i h_i(t) s(t - \frac{n_i}{N}T) e^{-j(\frac{2\pi}{T}t + \frac{2\pi n_i}{N} + \frac{\pi}{2})k'} \right] * f(t) \quad (2.13)$$

So, we compare the power computed via Monte-Carlo simulation to the Table estimated power (2.10). In our analysis, we have considered the PHYDYAS NPR (nearly perfect reconstruction) prototype filter using the frequency sampling technique with an overlapping factor  $K = 4$ [12], the other simulation parameters are shown in Table 2.1 and Table 2.2.

From Figure 2.4, we can see also that the Table estimation method still gives an accurate prediction of the power received in an asynchronous FBMC scenario. It can be noticed that, sometimes we have a slight difference between the Monte-Carlo method and the Table estimation power, this difference is due to the OQAM decision at the receiver (the offset of  $T/2$  between the real and the imaginary part).

## 2.3 Performance analysis of an uplink OFDM/FBMC multi-cell network

### 2.3.1 System Model

We consider the uplink of an unsynchronized cellular wireless network illustrated in Figure 2.5. The users in the neighboring cells transmit signals to their base stations. All the signals

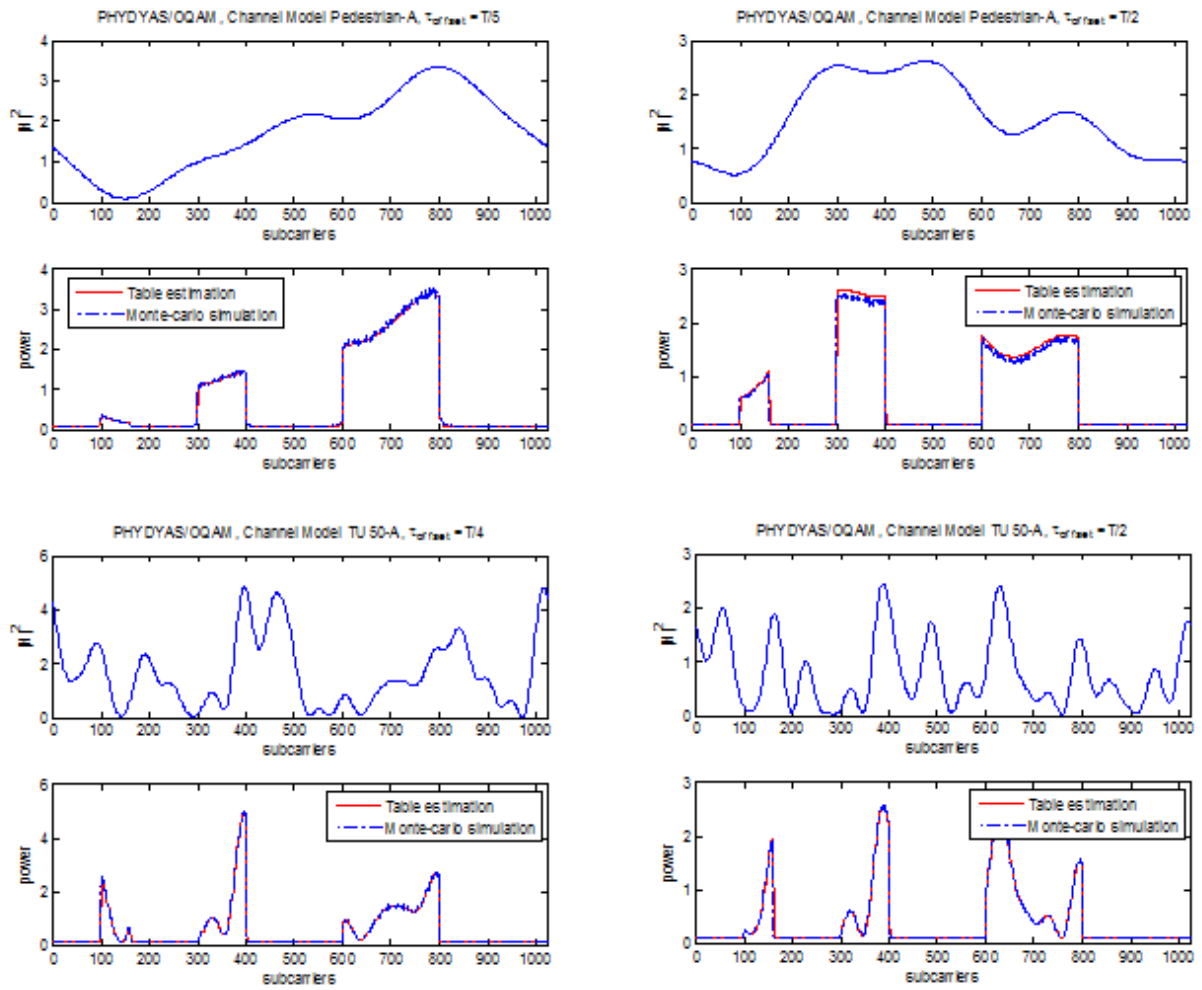


Figure 2.4: Table estimation and the Monte-Carlo comparison, FBMC case

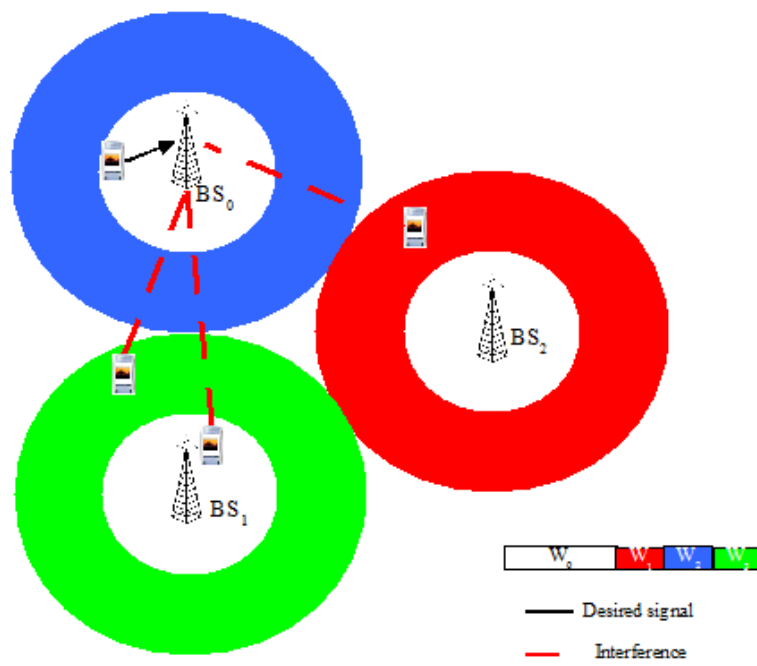


Figure 2.5: Uplink layout for a wireless cellular system

in Figure 2.5 propagate through multipath channels and are received at base station BS0. We assume that the propagation channels are stationary over the whole data frame. In each cell, all users are synchronized with their base stations but not necessarily synchronized with the BS(s) of the other cells.

### 2.3.1.1 Frequency reuse scheme

For a frequency reuse of 1, all subcarriers allocated to a cell can be used anywhere in the cell without any specification of the user's location. However, the reutilization of subcarriers in network cells may be one or greater. Therefore, the interference becomes more critical for the users located at the border area of the cell. To deal with this problem in OFDMA based system, several schemes of fractional frequency reuse (FFR) have been proposed [13, 14]. An example of FFR scenario is depicted in Fig. 2.6. As can be seen in the figure, cell area is divided into two regions, inner and outer. The FFR scheme suggests that the inner region of the neighboring cells share the same band, while their outer regions apply a frequency reuse factor of 3. The network bandwidth  $W$  is equal to  $W_0 + W_1 + W_2 + W_3$ . It is also considered that  $W_1 = W_2 = W_3$ . Hence, users located in the cell border mitigate the interference due to the frequency reuse factor of 3. By properly, adjusting the sizes of the inner and the outer regions, both capacity and the signal to interference ration (SIR) can be improved.

### 2.3.1.2 Network dimensioning

In order to specify the different parameters of the multi-cell network, we consider the scenario depicted in Figure 2.6. The distance between the reference user and its BS is equal to the distance between the interferer and its BS. Therefore the transmitted power is the same for both users ( $P_{Tx}$ ), the received power and the interference power are given by

$$P_{rec} = g_{b,u} P_{Tx} = A r^{-\gamma} P_{Tx} \quad (2.14)$$

$$I = g_{b,i} P_{Tx} = A (2R - r)^{-\gamma} P_{Tx} \quad (2.15)$$

where  $g_{b,u}$ ,  $g_{b,i}$ , denote the inverse of the pathloss between respectively (BS/ the reference user) and (BS/ interferer).  $\gamma$  is the pathloss exponent. Therefore, the signal to interference ratio SIR can be expressed as follows

$$SIR = \frac{P_{rec}}{I} = \left( \frac{2R - r}{r} \right)^{\gamma} \quad (2.16)$$

As aforementioned the bands of the outer regions are equals ( $W_1 = W_2 = W_3$ ). Then, we have just to specify the bandwidth of the inner region  $W_0$ . We assume that a scheduler guarantees throughput fairness among users of a cell and assuming that the users are uniformly distributed in the network, we have then

$$\frac{W_{i=1,2,3}}{W_0} = \frac{\pi(R^2 - r^2)}{\pi r^2} = \left( \frac{R}{r} \right)^2 - 1 \quad (2.17)$$

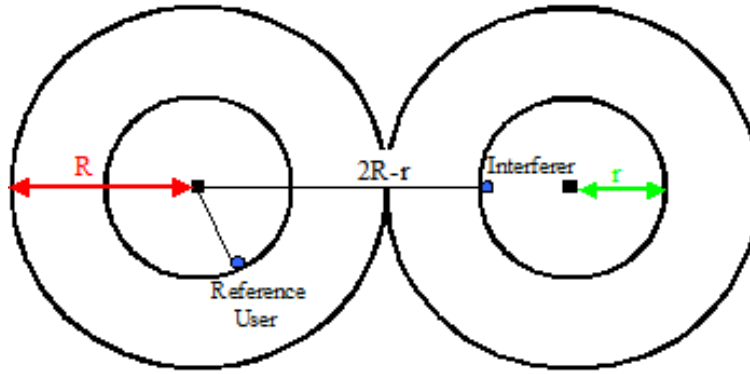


Figure 2.6: Cellular network with FFR worst case interference scenario

So, for a correct network dimensioning, we have to make sure that the two expressions (2.16) and (2.17) are satisfied.

### 2.3.2 Simulation

In this section, we compare the performance of CP-OFDM and FBMC in two simplified scenarios (A and B). In the first scenario A, we analyze the performance system when there is no overlapping between the desired signal frequency band (one reference user) and the interference frequency band (2 interferers) (see Figure 2.7-a). In the second one (scenario B), the interferers (3 users) are allowed to occupy the same frequency band of the desired signal (one reference user) (see Figure 2.7-b). Two cases are considered, interferer using the band of interest is close to the BS<sub>0</sub> or away from this latter.

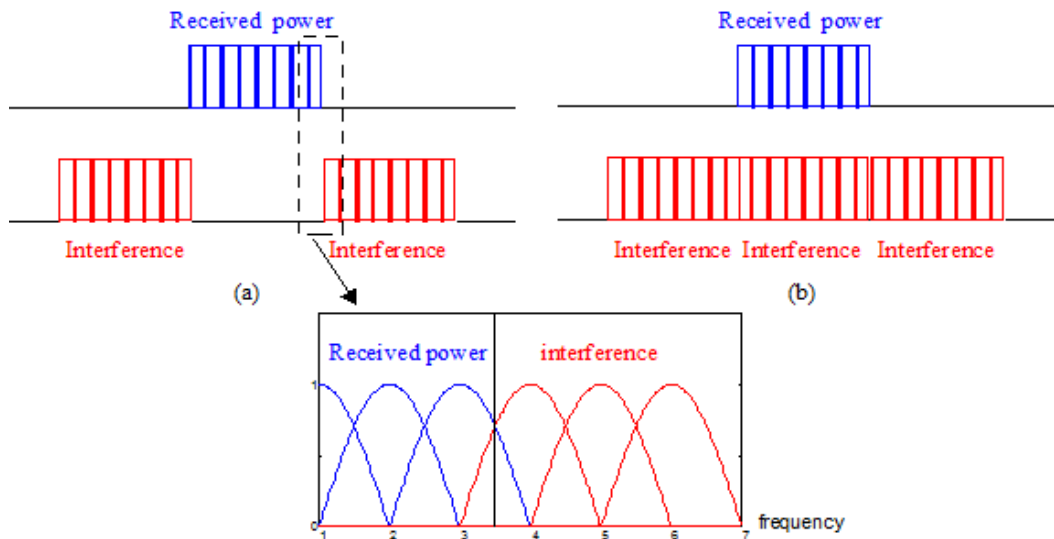


Figure 2.7: The two simplified scenarios A and B

The results have been obtained using the following parameters

Cell Parameters	
Number of cells	3
Cell Radius	1 km
Inner region radius	0.5 km
Antennas	SISO
OFDMA Parameters	
Total bandwidth	10 MHz
Carrier frequency	2.5 GHz
Number of subcarriers	1024
Number of subcarriers per cluster	18
Propagation Channel	
Channel model	TU50 model-A
Path Loss (dB)	$128.1 + 37.6 \log_{10}(d)$ ( $d$ in km) [15]
Power control	
PTx,max	20 dBm
Thermal Noise density	-174 dBm/Hz
SNR	20 dB

Table 2.3: Statistical simulation parameters

In the following results, we illustrate the interference plus noise power (IN), the SINR and the user capacity (C) of the system (CP-OFDM and FBMC). For each scenario, the evaluation of these parameters has been done using the Monte-Carlo simulation (MC) (averaged on the transmission of 1000 frames for each channel realization), the Table estimation method (TE) and also Perfect synchronized network case (PS). The average capacity of the reference user is given by

$$C_{\text{user}} = \frac{1}{K} \sum_{k \in B_{\text{user}}} \log_2[1 + \text{SINR}_k] \quad (2.18)$$

where  $B_{\text{user}}$  is the frequency band allocated to the user of reference,  $K$  is the number of subcarriers of  $B_{\text{user}}$ .

### 2.3.2.1 Scenario A

Figure 2.8 depicts the performance of CP-OFDM system in scenario-A for a cluster of 18 subcarriers, the simulation has been performed over 1000 independent channel realizations. We clearly see, that the capacity loss caused by the desynchronization is more than 20%. It should be noticed that we didn't take into account the CP factor in the capacity calculation which should reduce the computed capacity again by  $1/8=12.5\%$ . On the other hand, the results of FBMC in scenario-A are shown in Figure 2.9. We find that the FBMC system provides almost the same performance in both cases (the perfect synchronized network and the asynchronous one) except the two subcarriers of the borders which are affected by the interference. This can be explained by the good frequency localization of the PHYDYAS

prototype filter thus only immediate adjacent subcarriers are causing interference ( $k - 1$  and  $k + 1$ ).

$C_{\text{user}}[\text{bps/Hz}]$	OFDM	FBMC
Asynchronous case	5.27	6.37
Perfect synchronized case	6.65	6.65

Table 2.4: The user capacity of OFDM/FBMC in scenario A

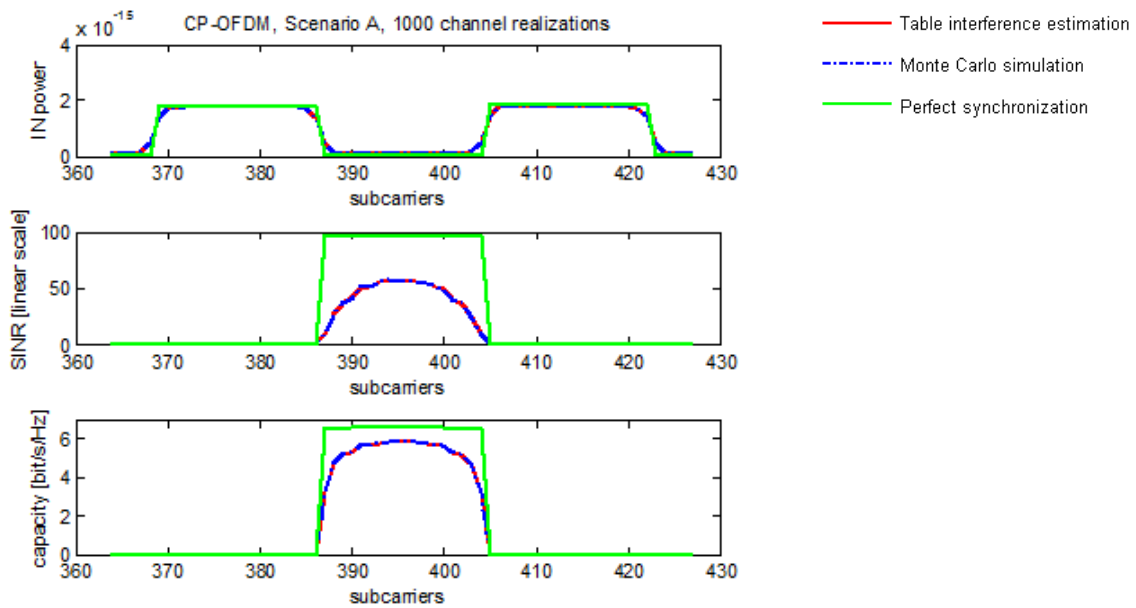


Figure 2.8: CP-OFDM performance in scenario A, cluster length =18 subcarriers (over  $10^3$  channel realizations)

### 2.3.2.2 Scenario B

In this scenario, as mentioned before there is another interferer which utilizes the sub-band of the reference user. We distinguish two cases: this interferer is close to the BS of interest (the corresponding results are depicted in Figure 2.10 and Figure 2.11 ) and when this interferer is far away from the BS of interest (the corresponding results are shown in Figure 2.12 and Figure 2.13). Through these results, we confirm and we validate all the observations noted in scenario-A. We see also that due to the network dimensioning, we can control the minimum SINR. From Figure 2.10 and Figure 2.11, the SINR is equal to 38.2 (15.8 dB); we can compute this SINR using (2.16) and the corresponding SINR is

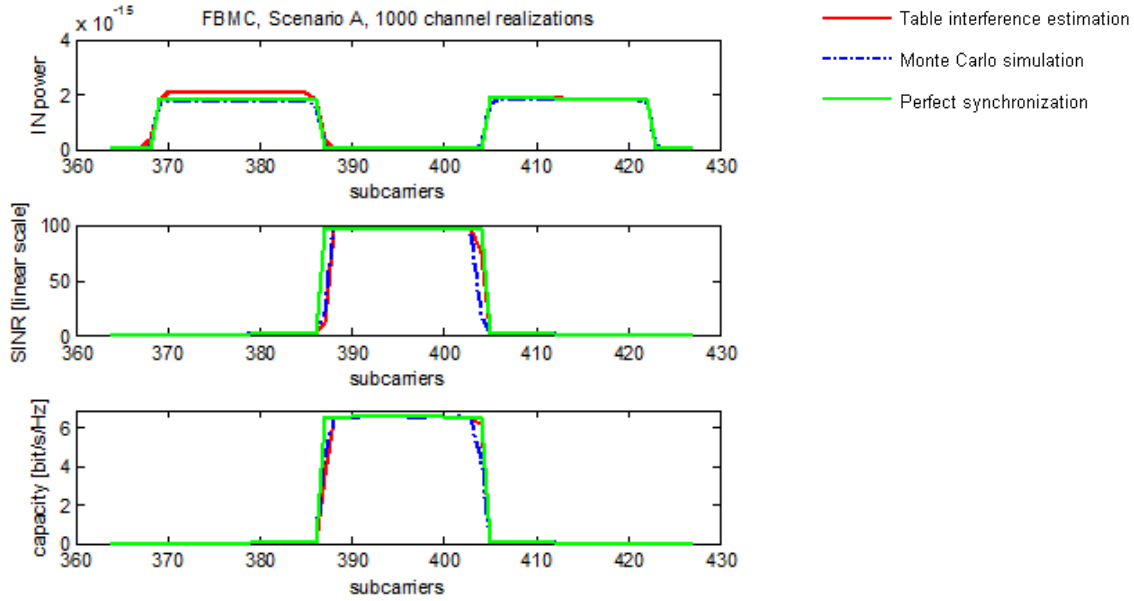


Figure 2.9: FBMC performance in scenario A, cluster length = 18 subcarriers (over  $10^3$  channel realizations)

given by

$$\text{SINR} = \frac{S}{I + N} = \frac{\text{SIRSNR}}{\text{SIR} + \text{SNR}} = 38.35(15.8\text{dB}) \quad (2.19)$$

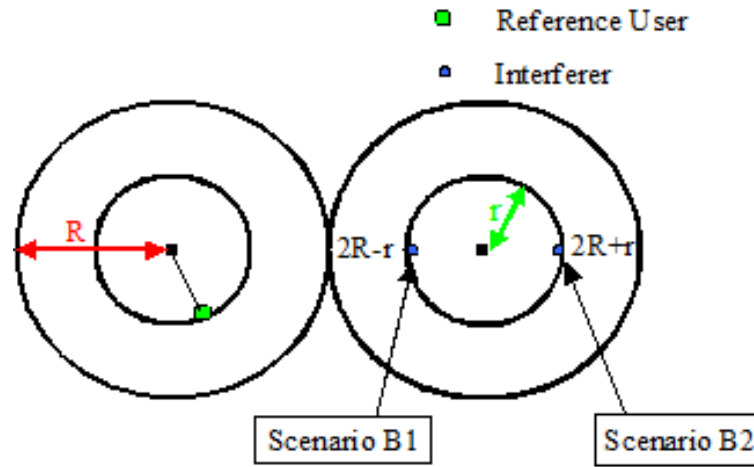
In the second situation (Scenario B2), as the interference coming from the same frequency band is affected by a strong attenuation (pathloss), and the SINR is equal to 19 dB.

It is worth noting that, the transmitted power of the adjacent bands (interferers located at a distance  $R$  of their BSs) is 23.76 times bigger than the transmitted power of the two users (reference user and the interferer using the frequency band of interest) which are located at a distance  $r$  of their BSs. Therefore, the perfect synchronized case still provide the best performance even in the presence of the interference coming from the same frequency band.

According to the results obtained in the scenario B, we can see that even when the interference comes from the same frequency band, the desynchronization remains an important factor which reduces the performance of the CP-OFDM system. We also notice that the FBMC system remains invulnerable to the desynchronization between the network cells. The capacity user for each situation is presented in Table 2.5.

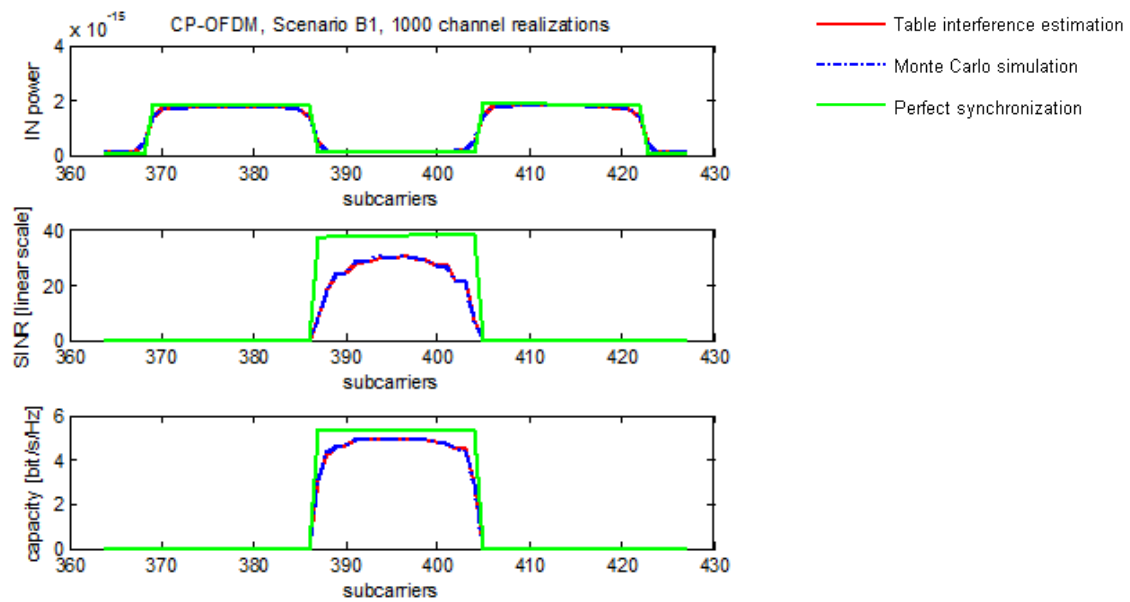
The accuracy of our model has been validated by the evaluation of the averaged capacity of the mobile user ( $\text{MU}_0$ ) considering the interference caused by  $\text{MU}_1$  which is not necessarily synchronized with the base station  $\text{BS}_0$  (see Fig. 2.3.2.2 and Fig. 2.3.2.2).





$C_{\text{user}}[\text{bps/Hz}]$	Scenario-B1		Scenario-B2	
	CP-OFDM	FBMC	CP-OFDM	FBMC
Asynchronous case	4.58	5.16	5.12	6.06
Perfect synchronized case	5.28	5.28	6.27	6.27

Table 2.5: The user capacity of OFDM/FBMC in scenario B

Figure 2.10: CP-OFDM performance in scenario B1, cluster length =18 subcarriers (over  $10^3$  channel realizations)

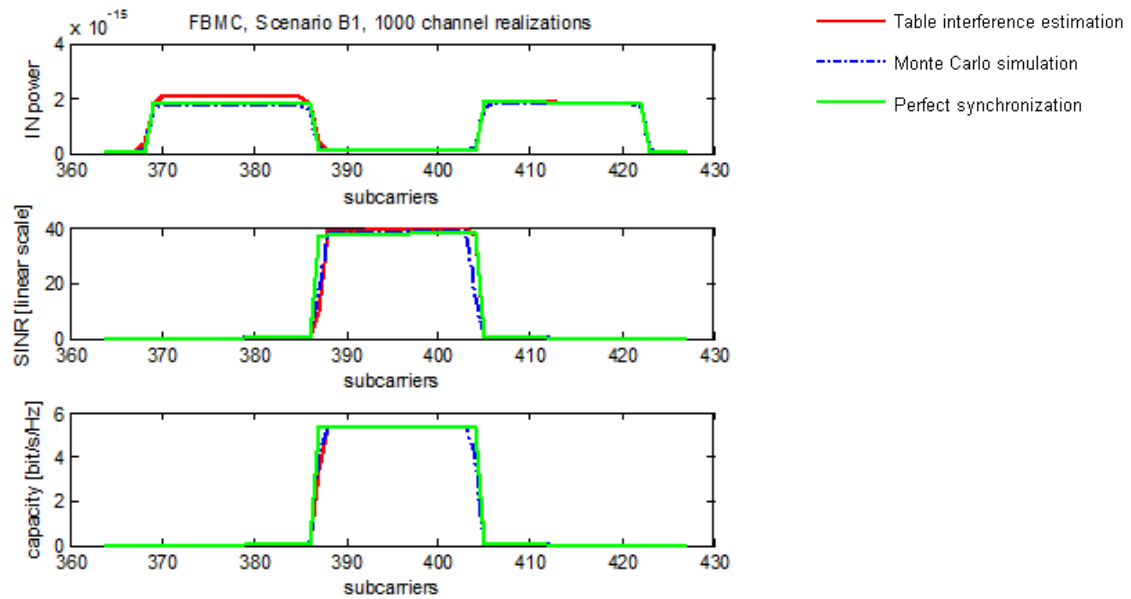


Figure 2.11: FBMC performance in scenario B1, cluster length =18 subcarriers (over  $10^3$  channel realizations)

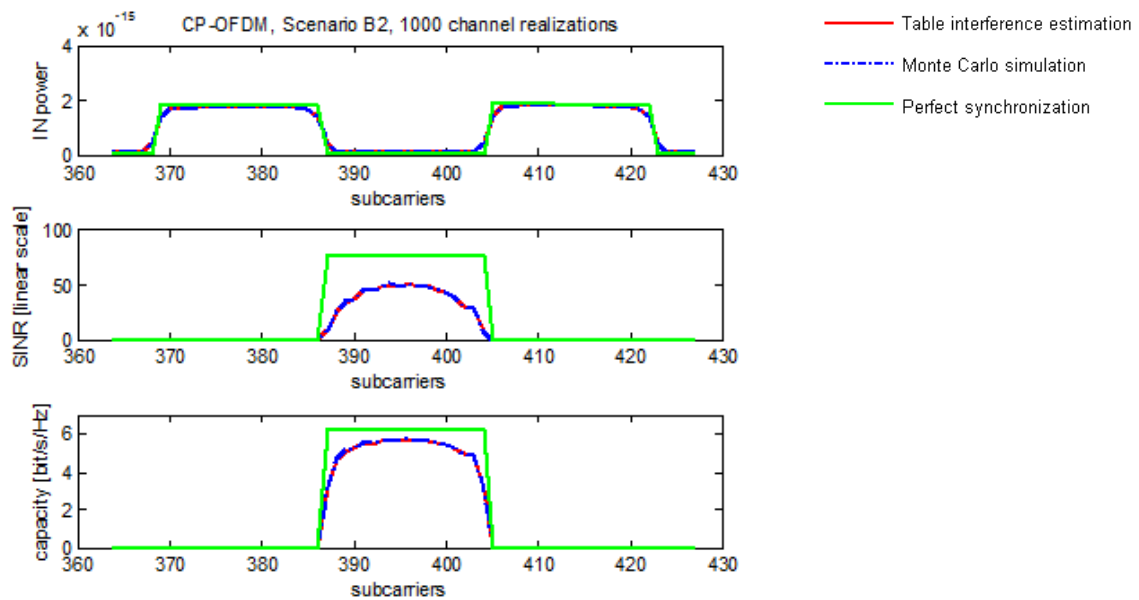


Figure 2.12: CP-OFDM performance in scenario B1, cluster length =18 subcarriers (over  $10^3$  channel realizations)

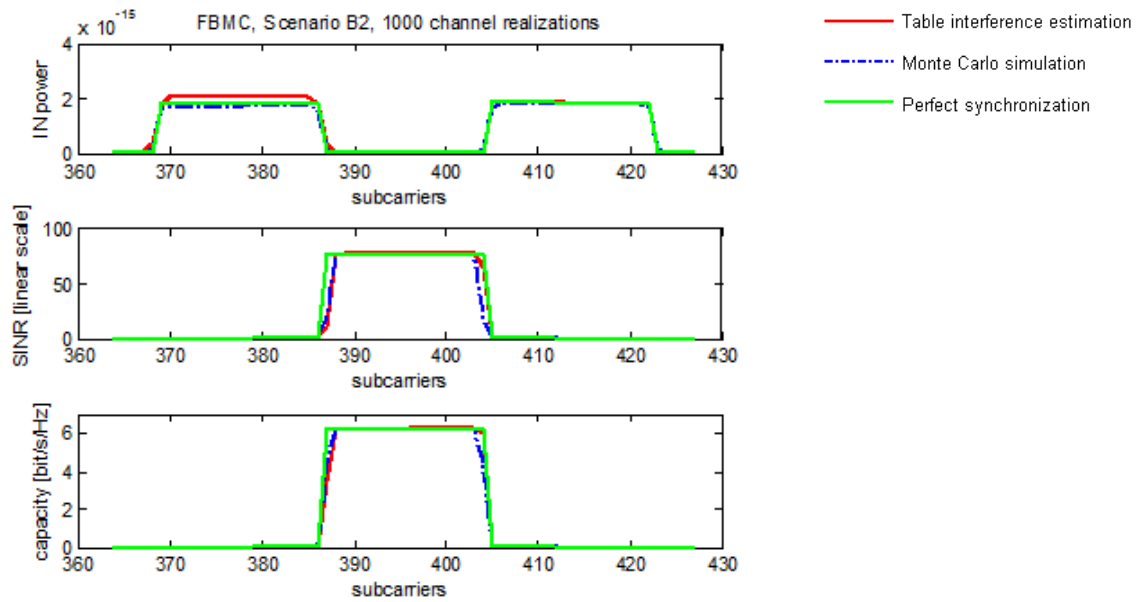


Figure 2.13: CP-OFDM performance in scenario B1, cluster length = 18 subcarriers (over  $10^3$  channel realizations)

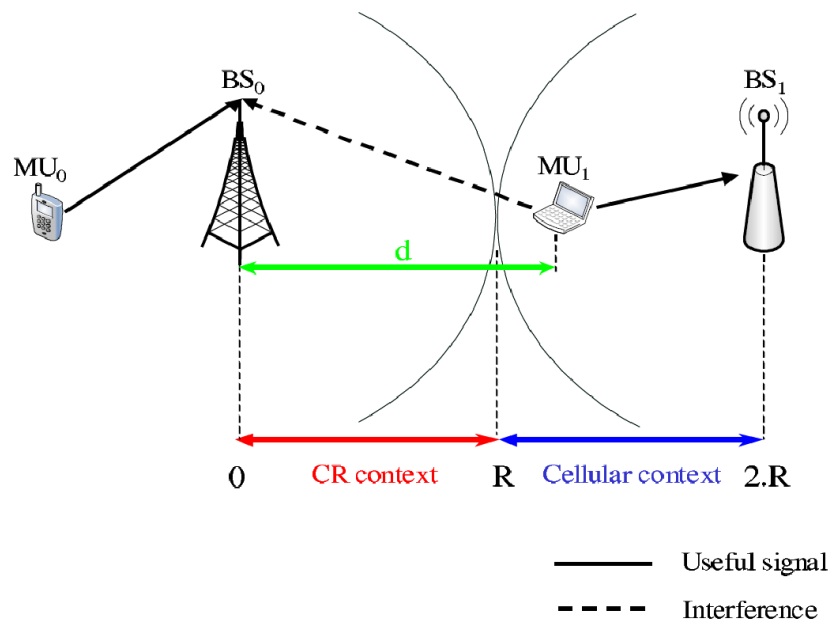


Figure 2.14: Interference model: the reference user coexists with an asynchronous interferer

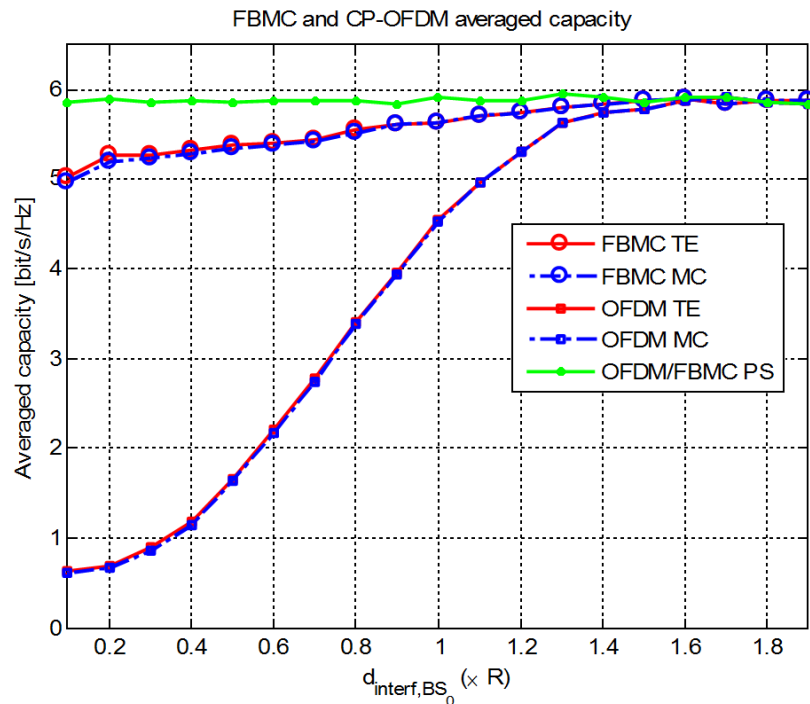


Figure 2.15: FBMC and OFDM averaged capacity vs. distance between  $MU_1$  and  $BS_0$

## 2.4 Conclusion

We have proposed an accurate method to estimate the interference caused by the imperfect inter-cell synchronization. This method is based on the interference Table introduced in [9] and it assumes only the knowledge of the channel power gain.

Part of this work has been published with more details in [11],[16]. A global evaluation of the performance in asynchronous OFDM/FBMC based multi-cellular networks has been performed and closed-form expressions of the BER have been developed in [17]. The interference tables have also been used to compare the spectral efficiency of OFDM/FBMC for uplink cognitive radio networks in [5].

The performance of the uplink of CP-OFDM and FBMC multi-cell network has been investigated. Through the different tests performed, we have illustrated that, the performance of CP-OFDM based network is prone to degradation when the cells are not synchronized (the orthogonality between subcarriers is damaged). However, the FBMC based multi-cell network is not vulnerable to the inter-cell desynchronization due to the good frequency localization of the prototype filter (only immediate adjacent subcarriers are causing interference). It is worth mentioning that in contrast to the direct evaluation method that requires huge computational efforts, the proposed method reduces significantly the computation complexity.

# Chapter 3

## Cross-layer design: resource allocation and scheduling methods

### 3.1 Uplink Resource Allocation in CP-OFDM and FBMC Systems

#### 3.1.1 Introduction

Resource allocation in the downlink of multicarrier systems has been discussed in [10] and [18], where we introduced our cross-layer system model, the heuristic allocation algorithm as well as simulation results obtained with both CP-OFDM and FBMC systems. At the resource allocator, the total transmit power that is required to fulfill given QoS constraints is minimized, and the FBMC system has been demonstrated to demand less transmit power than the CP-OFDM system with the same target QoS. What is more, a separated resource allocation and scheduling approach has also been designed, where for each *Transmission Time Interval* (TTI), the scheduler, which functions on top of the resource allocator, schedules the traffic from the end users and decides for a list of packets to be served in the current TTI and passes information about the list to the resource allocator. By performing the real resource allocation and comparing the minimized transmit power with the total available amount at the BS, the resource allocator determines whether the input packet list is servable or not. Therefore, as the FBMC system is more successful in serving given packet lists, it is able to satisfy the QoS requirements of more data streams from the end users (see simulation results provided in Sec. sec:ractire) as compared to the CP-OFDM system.

In this chapter, the uplink resource allocation problem is investigated. The same system model as employed for the downlink case is used, and similar research steps have been followed: we first develop a resource allocation algorithm for general multicarrier systems, which, like the downlink algorithm, effectively provides suboptimal solutions to the resource allocation problem. Then the effects of *carrier frequency offset* (CFO) on the two multicarrier systems in the uplink is studied, and methods for compensating the residual

CFO are discussed. Finally the allocation plus compensation procedure is applied to both systems such that comparative results can be obtained. We will see that the advantage of the FBMC system is even more obvious and crucial in the uplink than in the downlink regarding the efficiency and robustness of the resource allocation.

### 3.1.2 Uplink resource allocation algorithm

#### 3.1.2.1 Problem formulation

We directly start with the problem formulation as the system model employed is the same as described in [10] and [18]. In the multiuser uplink, each transmitter is constrained with a maximum transmit power. For mobile users, this number is usually rather limited. Assume that there are in total  $K$  users in the cell which have data to transmit to the BS in the current TTI. Let the number of information bits user  $k$  wants to transmit be  $b_k^{(\text{rq})}$ , the maximum latency allowed for the successful transmission be  $\tau_k^{(\text{rq})}$ , and the available transmit power be  $P_k^{(\text{av})}$ . The resource allocation problem is formulated here as minimizing the sum transmit power under individual transmit power constraints as well as the QoS requirements:

$$\begin{aligned} \min_{\mathbf{B} \in \mathcal{B}} \quad & \sum_{k=1}^K \sum_{n=1}^N P_{k,n}(B_{k,n}, \tau_k^{(\text{rq})}) \\ \text{s.t.} \quad & \sum_{n=1}^N B_{k,n} \geq b_k^{(\text{rq})}, \quad k = 1, \dots, K, \\ & \sum_{n=1}^N P_{k,n}(B_{k,n}, \tau_k^{(\text{rq})}) \leq P_k^{(\text{av})}, \quad k = 1, \dots, K, \end{aligned} \quad (3.1)$$

where  $\mathbf{B} \in \mathbb{Z}_{+,0}^{K \times N}$  represents the bit-loading matrix with its entry  $B_{k,n}$  as the number of information bits from the  $k$ th user loaded onto the  $n$ th subchannel, and  $P_{k,n}(B_{k,n}, \tau_k^{(\text{rq})})$  denotes the corresponding minimum transmit power required to successfully deliver  $B_{k,n}$  bits within latency  $\tau_k^{(\text{rq})}$ . The constraint  $\mathbf{B} \in \mathcal{B}$  comes from FDMA in which  $\mathcal{B} \subset \mathbb{Z}_{+,0}^{K \times N}$  represents the set of matrices that have only one nonzero entry in each of their columns.

For each loaded *minimum allocation unit* (MAU) which is defined as the two-dimensional region of one subchannel in frequency times one TTI in time, a *modulation and coding scheme* (MCS) can be chosen from a pre-determined candidate set  $\mathcal{M}$  whose elements are listed in Table 3.1. As a result, the maximum value  $B_{k,n}$  can take is limited by the highest MCS in  $\mathcal{M}$  and the number of data symbols in one MAU.

Also note that (3.1) is only one of the possible formulations of the uplink resource allocation problem. It is in fact a special case of the common formulation where each mobile user is given a weight value and the weighted sum transmit power is minimized. It will be clear in the following section that the algorithm we design to solve (3.1) is actually applicable to the more general weighted sum power minimization problems.

Table 3.1: Modulation and Coding Schemes (MCS)

Index	Modulation Type	Alphabet Size $A$	Code Rate $R$	$R \log_2 A$
1	BPSK	2	1/2	0.5
2	QPSK	4	1/2	1
3	QPSK	4	3/4	1.5
4	16-QAM	16	1/2	2
5	16-QAM	16	3/4	3
6	64-QAM	64	2/3	4
7	64-QAM	64	3/4	4.5
8	64-QAM	64	5/6	5

### 3.1.2.2 Branch and bound algorithm

Due to the exclusive assignment of an MAU to only one user and the limited discrete MCS that can be chosen, (3.1) is a combinatorial optimization with NP complexity. Recall that we proposed a stepwise approach to solve the downlink resource allocation problem in the previous deliverables, namely, a *subchannel assignment* (SA) is firstly found where the same MCS is assumed for one user, and then *bit and power allocation* (BPA) is performed based on the obtained SA. This approach is not quite suitable for the uplink problem, for the individual power constraints also have to be taken into account in the SA step. In solving the downlink resource allocation problem, SA has been shown to be crucial to the performance of the algorithm; in the uplink case, SA is even more important as it determines whether a feasible solution can be found. Therefore, we propose a new algorithm to deal with the uplink resource allocation problem.

The *branch and bound* (BAB) algorithm is one of the most commonly used integer programming methods [19]. Being an enumeration method in essence, it promises to give the global optimal solution irrespective to the convexity of the problem. Yet the convergence speed depends on many factors and is hard to predict. To reduce the number of variables, we make the assumption first that each MAU is fully loaded, *i.e.*, all data symbols in an MAU are occupied. Base on that,  $K$  matrices of dimension  $|\mathcal{M}| \times N$  and 0 – 1 elements can be used to indicate which MCS is used on which subchannel by which user. Let such a matrix for user  $k$  be  $\mathbf{X}^{(k)}$ .  $X_{m,n}^{(k)} = 1$  then means that the  $m$ th MCS is employed on subchannel  $n$  by user  $k$ . If all  $K$  matrices are stacked together, we obtain the matrix  $\mathbf{X}$  as

$$\mathbf{X} = \begin{bmatrix} \mathbf{X}^{(1)} \\ \vdots \\ \mathbf{X}^{(K)} \end{bmatrix}$$

which we call the *selection matrix*. Correspondingly, the values of transmit power that are required to support the respective transmissions are computed and stored in the *power*

matrix

$$\mathbf{P} = \begin{bmatrix} \mathbf{P}^{(1)} \\ \vdots \\ \mathbf{P}^{(K)} \end{bmatrix}.$$

With these notations, (3.1) is transformed into the following problem:

$$\begin{aligned} \min_{\mathbf{X} \in \{0,1\}^{K|\mathcal{M}| \times N}} \quad & \text{tr}(\mathbf{P}^T \mathbf{X}) \\ \text{s.t.} \quad & \sum_{m=1}^{K|\mathcal{M}|} X_{m,n} \leq 1, \quad n = 1, \dots, N, \\ & \mathbf{b}^T \mathbf{X}^{(k)} \mathbf{1} \geq b_k^{(\text{rq})}, \quad k = 1, \dots, K, \\ & \text{tr}(\mathbf{P}^{(k)T} \mathbf{X}^{(k)}) \leq P_k^{(\text{av})}, \quad k = 1, \dots, K, \end{aligned} \quad (3.2)$$

where  $\mathbf{b}$  is the column vector of  $|\mathcal{M}| \times 1$  containing the numbers of information bits when each MCS is used, and  $\mathbf{1}$  is the column vector of all 1 entries. We denote the optimum value of (3.2) by  $P_{\min}$ .

Problem (3.2) can be solved using the BAB algorithm specialized for the 0-1 problems, *i.e.*, problems in which the variables can only be 0 or 1. A summary of the algorithm is given in Algorithm 1 and explained in the following.

---

**Algorithm 1** Branch and bound algorithm

---

- 1: Solve the *linear programming relaxation* (LPR) of (3.2) by using any standard algorithm
  - 2: Terminate if LPR of (3.2) is infeasible
  - 3: Compute the global upper and lower bound  $U$  and  $L$  on  $P_{\min}$
  - 4: Terminate if  $\frac{U-L}{L} < \epsilon$
  - 5: Select a fractional variable  $x$  and create two branches by setting  $x = 0$  and  $x = 1$
  - 6: Solve the LPR's of the two branches and compute the respective upper and lower bounds
  - 7: Update the global upper and lower bound if necessary
  - 8: Terminate if  $\frac{U-L}{L} < \epsilon$
  - 9: Choose the branch with lower LPR objective and repeat steps 5–8
- 

If the elements of the selection matrix  $\mathbf{X}$  can take values between 0 and 1 instead of only 0 and 1, (3.2) becomes a linear optimization that can be solved by any standard linear optimizer, and the optimal value of this relaxed problem provides a lower bound on  $P_{\min}$ , as its domain is larger than (3.2). Note that if the relaxed problem is infeasible, (3.2) can be determined to be infeasible. As any feasible solution to (3.2) provides an upper bound on the problem, at each branch, we try to recover a feasible solution based on the fractional solution to the LPR. A heuristic algorithm is designed to accomplish this.

If the number of fractional, *i.e.*, non-integer, variables in the LPR solution is very small, all possible combinations of them can be enumerated and the one that leads to the minimum sum power is taken. If this is not the case, we can find the set of subchannels



that are shared by different users and determine the owners of these subchannels according to the fractions each user get on them as well as how important they are to each user. For example, if a user only holds a fraction of one particular subchannel and no other subchannels, this subchannel has to be assigned to the user; without such special conditions a shared subchannel is assigned to the user with the largest fraction of it. After one shared subchannel is assigned, the reduced LPR is resolved and the procedure repeats until there are no more shared subchannels. Although performing well in many cases as we can see with the simulation results shown in the next subsection, it should be noted that this recovery is by no means optimal and does not guarantee to provide a feasible solution.

If the difference between the global upper and lower bounds we obtain is small enough with respect to the lower bound, *i.e.*, the ratio between the two is below a pre-defined threshold  $\epsilon$ , the best feasible solution so far is proven optimal, and the BAB algorithm terminates. Otherwise, the branch with lower LPR objective is chosen to be further branched. The BAB algorithm is implemented recursively and requires a lot of memory when executed. At each node in the BAB tree, at least one linear optimization is solved. Also note that the adaptive subchannel size scheme discussed in [18] is employed which iteratively calls the resource allocation algorithm and thus requires a certain degree of efficiency and speed of the algorithm.

### 3.1.2.3 Simulation results: validation of the algorithms

To justify the correctness of the BAB algorithm and the efficiency of the heuristic recovery algorithm, a few simple tests have been performed for which the detailed parameters are listed in Table 3.2 (for other system and simulation parameters [18] should be referred to). Here we fix the subchannel size to  $N_c = 24$  and the number of symbols in one TTI to  $N_s = 18$ . For each test, resource allocation is performed under 1000 independent channel realizations and the results are shown in Fig. 3.1.

Table 3.2: Test parameters

Test 1				Test 2			
$k$	$b_k^{(\text{rq})}/\text{bits}$	$\tau_k^{(\text{rq})}/\text{ms}$	$P_k^{(\text{av})}/\text{mW}$	$k$	$b_k^{(\text{rq})}/\text{bits}$	$\tau_k^{(\text{rq})}/\text{ms}$	$P_k^{(\text{av})}/\text{mW}$
1	512	20	200	1	512	20	200
2	800	50	400	2	400	50	200
				3	800	50	400

In the first test, we assume that there are 2 users in the cell and only 4 subchannels. In this case there are in total 50 combinations of SA and MCS selection that could fulfill the QoS requirements, *i.e.*,  $\mathbf{X}$  has 50 different possibilities, which is tolerable for enumeration. Besides the global optimal objective found by the BAB algorithm ( $\epsilon = 0.05$  is used for the stopping criteria), we also record the global upper bound obtained by the heuristic recovery algorithm at the root node of the BAB tree. Simulation results indicate that

the optimum obtained with enumeration is always identical to the one found by the BAB algorithm. Out of the 833 simulated cases for which the problem is found feasible, there are 14 cases in which no feasible solution is found at the root node of the BAB tree. For the rest simulations, the root node objective is 0.2161 dBm larger than the optimum on average.

In the second test 3 users and 8 subchannels are assumed. To enumerate all possible  $\mathbf{X}$  is not practical in this case, yet the BAB algorithm can still provide the optimum solution in reasonable time. The efficiency of the heuristic algorithm is again demonstrated in that a feasible solution is recovered in 98.7% of all cases from the fractional solution given by the LPR of the problem, and the objectives associated with these solutions are only 0.1367 dBm worse on average than the optimal objectives. This suggests that in a system with even more users and subchannels for which the BAB algorithm takes too long to find the optimal solution, the heuristic algorithm can be effectively employed to provide a suboptimal solution.

### 3.1.3 Effects and compensation of CFO in the uplink

In [18] we studied the effects of CFO on both CP-OFDM and FBMC systems in the downlink. The computation of the intercarrier and intersymbol interference as well as the SINR remains basically the same in the uplink. Yet the CFO between each mobile user and the BS can be very different, which causes perfect synchronization at the BS to be practically impossible. For a subcarrier whose immediate neighboring subcarrier is used by another user as itself, the worst case interference can be significant which leads to a severe SNR degradation. Besides the power compensation method introduced in [18], we also discuss the scheme of leaving one or more subcarriers free at the edge of each subchannel to combat the effects of residual CFO.

#### 3.1.3.1 Effects of CFO

With the presence of CFO, the signal power on the desired subcarrier is attenuated and a fraction of the signal power on other subcarriers or symbols becomes interference to the desired signal. Unlike in the downlink where there is only one CFO between the subcarriers at the transmitter and the receiver, in the uplink, there could be  $K$  different CFO's between the corresponding subcarriers, where  $K$  is the number of mobile users. This means that the way each subcarrier influences other subcarriers is different, depending on the CFO as well as the channel condition between the user transmitting on it and the BS. As has been shown in [18] and other related literature, the immediately adjacent subcarriers contribute to the most significant part of the interference. Therefore, we are interested in the edge or boundary subcarriers in a subchannel, for their neighbors may have a very different CFO as themselves.

Let the residual CFO between any MS and the BS satisfy  $\varepsilon \in [-\varepsilon_{\max}, \varepsilon_{\max}]$ . This synchronization precision can be achieved by CFO estimation and compensation schemes employed at the BS and also by feedback of the CFO estimation to the MS and the

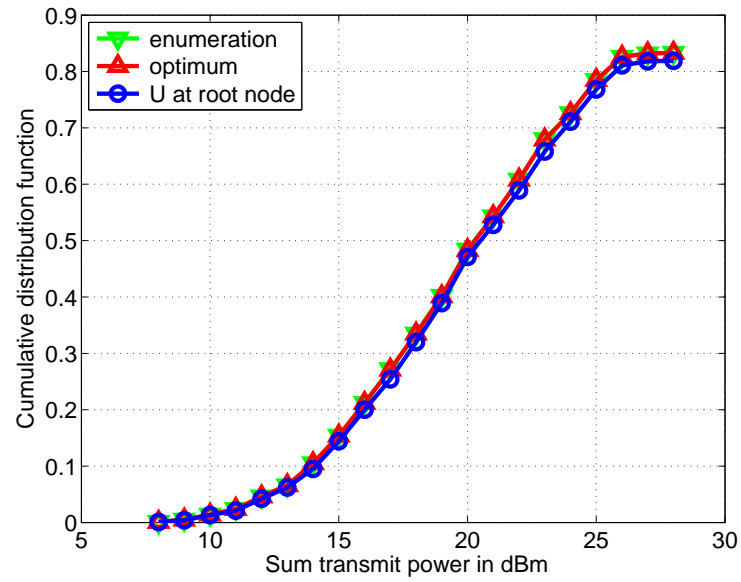
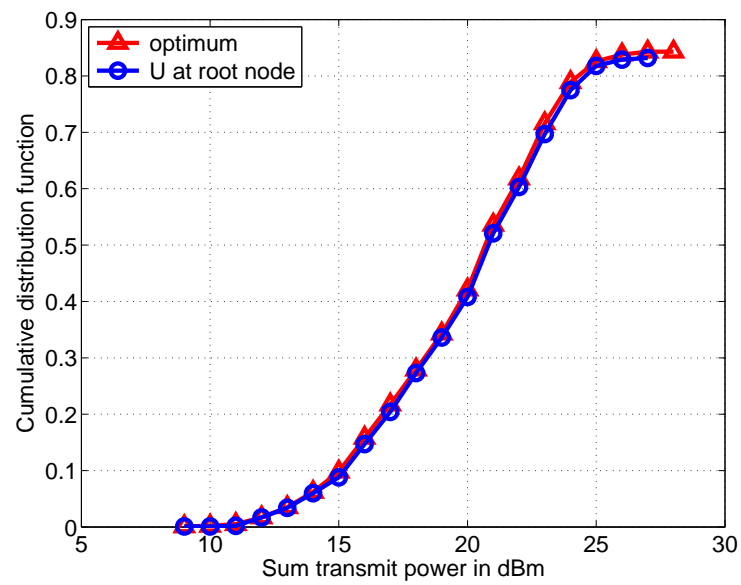
(a) Test 1:  $K = 2$ ,  $N = 4$ (b) Test 2:  $K = 3$ ,  $N = 8$ 

Figure 3.1: CDF of minimum sum transmit power

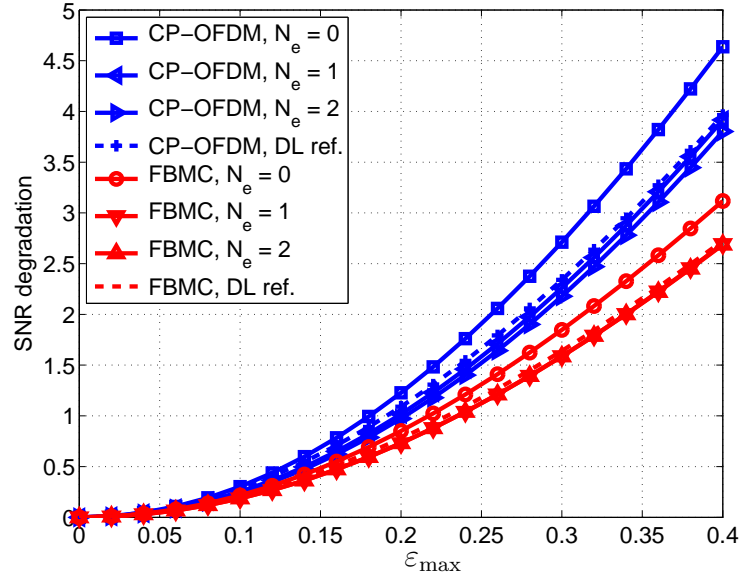
adjustments done at the MS. For a subcarrier at the left boundary of a subchannel, maximal SNR degradation is caused by the situation that all subcarriers on its right has the CFO  $-\varepsilon_{\max}$ , while all subcarriers on its left has the CFO  $\varepsilon_{\max}$ . The SNR degradation in this worst case dependent on  $\varepsilon_{\max}$  is numerically computed and illustrated in Fig. 3.2(a) with the solid curves labeled by  $N_e = 0$ , where the channel is assumed to be AWGN, the power allocation on the subcarriers is assumed uniform and the SNR without CFO equals 0 dB. The corresponding downlink case, *i.e.*, all subcarriers have CFO  $\varepsilon_{\max}$ , is drawn in dotted lines as a reference (DL ref), which helps emphasize the substantial impact of CFO in the uplink of multicarrier systems. Here  $N_e$  denotes the number of subcarriers that are left empty at the edge of a subchannel. As can be seen from the figure, when one edge subcarrier is left empty, the SNR degradation is significantly reduced for both CP-OFDM and FBMC systems. Leaving two subcarriers empty further improves the robustness of CP-OFDM, but the impact on FBMC system is almost negligible.

For comparison purpose, we also compute and draw in Fig. 3.2(b) the average SNR degradation of a boundary subcarrier under the same assumptions except that the CFO of each subchannel is a random number which is uniformly distributed over  $[-\varepsilon_{\max}, \varepsilon_{\max}]$ . Although the SNR degradation is obviously lessened in both systems, the advantage of the FBMC system is still apparent and the impact of leaving one or two boundary subcarriers empty is similar as in the worst case.

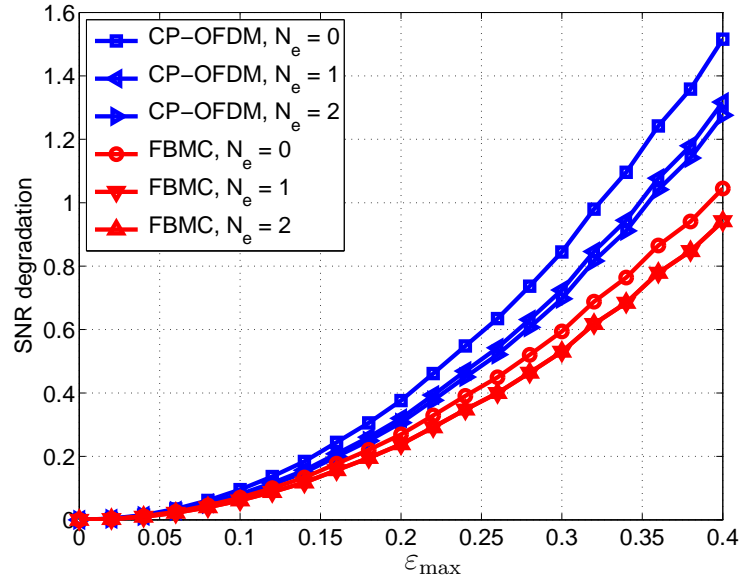
### 3.1.3.2 Compensation of CFO

In the downlink resource allocation procedure, we compensated for the worst case residual CFO by solving a set of linear equations on the power allocated on each subcarrier, where the linear coupling between the subcarriers is represented by the off-diagonal elements of the matrix containing the coefficients of the equation system. If the CFO is sufficiently large, the solution obtained could have negative entries indicating that the required SINR values on the subcarriers are not feasible, which means that the resource allocation has failed. Such a situation happens more often in the uplink due to the worse CFO and interference condition. What is more, even if the power vector obtained has only nonnegative entries, it could well violate the transmit power constraints of some users since more power is required to achieve the given SINR as compared with the zero CFO case. In a word, there is a good chance in the uplink that the CFO would cause the optimized resource allocation strategy to fail in providing the target QoS.

To avoid this, many conservative methods can be used, for example, to leave a margin of the transmit power for each user when performing the resource allocation optimization, or to leave a few boundary subcarriers empty which has been tested in this work. These methods would result in an inefficient utilization of the radio resources and yet do not guarantee a successful resource allocation since there is only statistical knowledge of the CFO's present in the system. Another small trick that can be applied is on the arrangement of information bits in a MAU. Recall that in Sec. 3.1.2, we reduce the problem (3.1) to (3.2) by assuming that each MAU is fully loaded. After the optimal or suboptimal solution is computed for (3.2), there are usually a number of extra bits that could be taken off from



(a) Worst case SNR degradation of a boundary subcarrier



(b) Average SNR degradation of a boundary subcarrier

Figure 3.2: SNR degradations vs.  $\varepsilon_{\max}$  in CP-OFDM and FBMC systems with AWGN channel and SNR = 0 dB

each user. With the objective to diminish the effect of CFO, the unload of extra bits can be done such that the number of MAU's which could have one subcarrier empty is maximized. The actual unload with a given selection matrix  $\mathbf{X}$  should also depend on the MCS chosen on the MAU's and on whether the neighboring subchannel is assigned or not.

### 3.1.4 Simulation results and analysis

The system parameters used for simulations are mostly the same as those listed in [18]. We only list the different parameters of the two systems in Table 3.3 to emphasize the reason for the better performance of the FBMC system. Due to the less out-of-band emission it generates and the absence of CP, the FBMC system can employ more subcarriers (5% more than CP-OFDM is assumed) and more symbols per TTI (12.5% more than CP-OFDM is assumed which is a common fraction of CP to the number of data samples) for data transmission.

Table 3.3: Parameter differences of CP-OFDM and FBMC systems

Number of data subcarriers in OFDM	$N_d$	720
Number of data subcarriers in FBMC	$N_d$	756
Number of data symbols per TTI in OFDM	$N_s$	16
Number of data symbols per TTI in FBMC	$N_s$	18

The designed users' QoS requirements and transmit power constraints are listed in Table 3.4.

Table 3.4: Users' QoS requirements and transmit power constraints

$k$	$b_k^{(\text{rq})}/\text{bits}$	$\tau_k^{(\text{rq})}/\text{ms}$	$P_k^{(\text{av})}/\text{mW}$	$k$	$b_k^{(\text{rq})}/\text{bits}$	$\tau_k^{(\text{rq})}/\text{ms}$	$P_k^{(\text{av})}/\text{mW}$
1	512	20	100	5	400	40	200
2	512	20	100	6	800	40	200
3	400	20	100	7	800	50	300
4	400	20	200	8	800	50	300

As the scale of the resource allocation problem is relatively large, the heuristic algorithm is used in each allocation instead of the BAB algorithm. We first test the scheme where no subcarrier is forced to be left empty in an MAU. In the 1000 simulations performed for  $\varepsilon_{\max} = 0.05$ , the CP-OFDM system declares that the resource allocation problem in 325 simulations are infeasible, but produces only 611 successful allocations, which means that in the remaining 64 simulations the algorithm can neither determine the problem is infeasible nor give a feasible allocation. The FBMC system on the other hand, only finds the allocation problem in 245 simulations infeasible and produces 719 successful allocations,

leaving only 36 undetermined cases. When  $\varepsilon_{\max}$  is increased to 0.1, the algorithm fails in 7 simulations to compensate for the residual CFO in the CP-OFDM system, which does not happen at all with the FBMC system.

Besides the lower outage ratio and higher robustness it presents, the FBMC system is also able to support the required QoS with less sum transmit power. In the simulations where both systems provide a feasible resource allocation, the FBMC system uses 0.6367, 0.6612, and 0.7483 dBm less transmit power on average corresponding to the maximum residual CFO values  $\varepsilon_{\max} = 0, 0.05, 0.1$ .

Secondly we test the scheme where one edge subcarrier in each subchannel is always left empty. By comparing the CDF of the minimum sum transmit power in this case which is drawn in Fig. 3.3(b) with the one obtained with the first test which is drawn in Fig. 3.3(a), one can quickly find out that the performance has been degraded. Take the FBMC system as an example. In the 1000 simulations performed, 283 are found infeasible which is 15.5% more than in the  $f_s = 0$  case. The reason for this degradation is that since data can not be loaded on the boundary subcarriers, they have to be squeezed into other subcarriers which means higher MCS are required which demand more transmit power. In all, the loss of the data transmission ability of these boundary subcarriers outcounts the potential savings from the residual CFO compensation, which renders the “empty subcarrier” scheme unfavorable, at least with the tested system and user parameters and  $\varepsilon_{\max}$  values.

### 3.1.5 Conclusions

In this section we have presented our recent work on the uplink resource allocation algorithms in general multicarrier systems and comparative studies on CP-OFDM and FBMC systems in the uplink. We first introduced the formulation of the resource allocation problem in the uplink, and then described the BAB algorithm which can be applied to obtain the optimal solution of the problem. A heuristic algorithm to recover feasible solutions at each node of the BAB tree was proposed which is not only an important part of the BAB algorithm, but also provides suboptimal solutions to the resource allocation problem and is thus very useful when the scale of the problem is large or the execution time is limited. Simulation results proved the effectiveness of the heuristic algorithm. In the second subsection we presented the effects of CFO in the uplink of CP-OFDM and FBMC systems where we see with numerical results that the uplink SNR degradations in the worst case can be extremely destructive, and discussed shortly about the methods to compensate for the residual CFO. At last simulation results have been shown which, on the one hand, validate the resource allocation procedure that has been designed, and on the other hand, demonstrate again that the FBMC system is more efficient and robust than the CP-OFDM system from a QoS provisioning and resource allocation point of view.

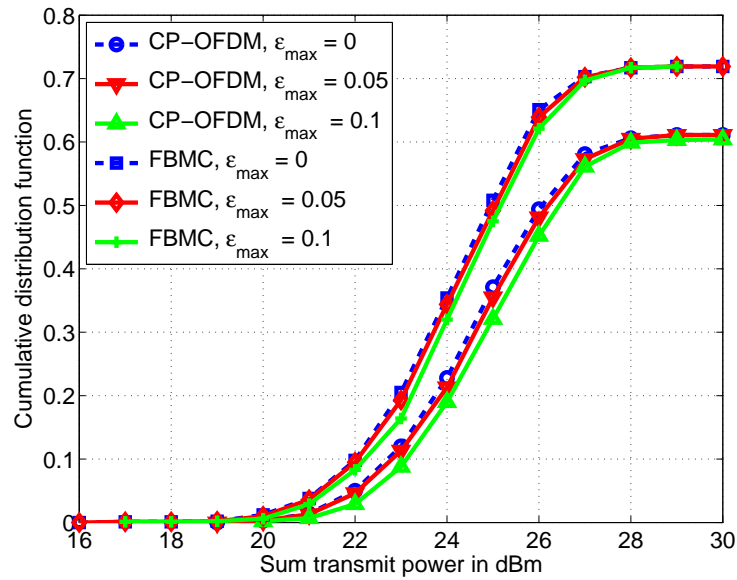
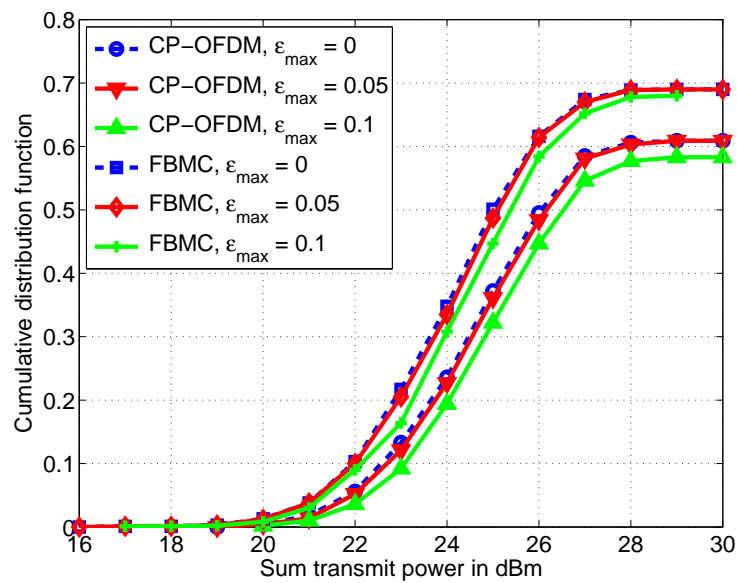
(a)  $N_e = 0$ (b)  $N_e = 1$ 

Figure 3.3: CDF of the minimum sum transmit power from 1000 simulations



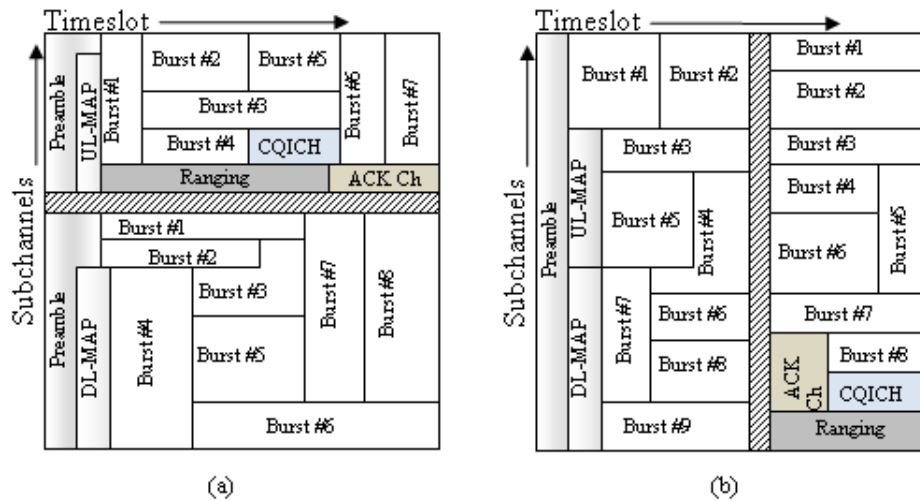


Figure 3.4: WiMAX frame structure for FDD (a) and TDD (b) mode

## 3.2 Scheduler description and results

### 3.2.1 System description

The system architecture of WiMAX consists of Base Stations (BSs), each one responsible for a specific area cell, and stationary Subscriber Stations (SSs). Two operation modes are defined: Point-to-Multipoint (PMP), for communication between the BS and the SSs of its cell, and Mesh mode for direct SS-to-SS communications without the need of a BS. At the PMP mode, each BS regulates all the communication in its cell. The communication path between SS and BS has two directions: uplink (from SS to BS) and downlink (from BS to SS), multiplexed either with Time Division Duplex (TDD) or Frequency Division Duplex (FDD). The communication between the BS and the SSs follows a frame by frame basis where each frame formatted by the BS consisting of the Downlink and the Uplink subframe (DL-subframe and UL-subframe) as it is shown in Fig. 3.4.

The DL subframe begins with a DL preamble, aiming to support PHY and MAC layer functionalities, such as time and frequency synchronization and channel estimation. A frame control header (FCH), providing frame configuration information, such as the modulation and coding scheme, and the usable subcarriers, follows this DL preamble. In addition, the data regions assigned to each user are broadcasted in the uplink and downlink MAP messages (UL-MAP and DL-MAP) after the FCH field. The frame size varying from 2 ms to 20 ms, however the current WiMAX equipment mainly supports 5ms frames. The DL subframe consists of multiple bursts with variable size and type dynamically distributed in time and frequency domain. Multiple concatenated packets or fragments of packets from upper layers are included in each burst. Similarly, the UL subframe consists of multiple bursts, however a portion is set aside for contention based

access usually called *ranging channel*. This portion is used for many purposes including network entry, close power control loop and bandwidth requests. Additionally, the uplink subframe includes a *channel-quality indicator channel* (CQICH) that used for the SS to feedback channel-quality information and an *acknowledgment channel* (ACK channel) to feed back downlink acknowledgments.

Multiple communication services are supported by WiMAX systems including data, voice, video, etc. Each connection in WiMAX systems represented by a Connection Identifier (CID) and characterized by service flow ID (SFID) that represents the set of Quality of Service (QoS) and traffic parameters that this connection requires. Five different classes of services are defined in IEEE 802.16 standard [20], depicted in Tab. 3.5:

Table 3.5: QoS classification

QoS category	Application	Specification
UGS	VoIP	maximum sustained traffic rate maximum latency tolerated jitter
rtPS	Video or Audio streaming	maximum sustained traffic rate minimum reserved traffic rate maximum latency traffic priority
ErtPS	VoIP with silence suppression	maximum sustained traffic rate minimum reserved traffic rate maximum latency tolerated jitter traffic priority
ntrPS	File Transfer Protocol	maximum sustained traffic rate minimum reserved traffic rate traffic priority
BE	Data Transfer, Web Browsing	maximum sustained traffic rate traffic priority

A scheduling algorithm located at the BS is responsible of maintaining the parameters of each service class. This scheduling decides for the resource allocation in each time frame. Uplink scheduling is performed by the BS with the aim of providing each Subscriber Station (SS) with enough bandwidth for uplink transmissions or opportunities for extra transmission requests. When additional bandwidth is needed, the SS utilizes its transmission opportunities during contention periods or when it is polled by the BS, depending on its agreed QoS characteristics, to pass its transmission requests. Downlink scheduling on the other hand, considers packets waiting for transmission at the BS as implicit requests for bandwidth allocation.

The scheduler has to combine the following properties:

*Fast Data Scheduling:* The MAC scheduler must efficiently allocate available resources in response to bursty data traffic and time-varying channel conditions. The scheduler is located at each BS to enable rapid response to traffic requirements and channel conditions.

*Scheduling for both DL and UL:* The scheduling service is provided for both DL and UL traffic. In order for the MAC scheduler to make an efficient resource allocation and provide the desired QoS in the DL, the UL must feedback accurate and timely information as to the traffic conditions and QoS requirements. Multiple uplink bandwidth request mechanisms, such as bandwidth request through ranging channel, piggyback request and polling are designed to support UL bandwidth requests. The UL service flow defines the feedback mechanism for each uplink connection to ensure predictable UL scheduler behavior.

*Dynamic Resource Allocation:* The MAC supports frequency-time resource allocation (in both DL and UL) on a per-frame basis. The resource allocation is delivered in MAP messages at the beginning of each frame and can be changed frame-by-frame in response to traffic and channel conditions.

*QoS Oriented:* The MAC scheduler handles data transport on a connection-by-connection basis. Each connection is associated with a single data service with a set of QoS parameters that quantify the aspects of its behavior. With the ability to dynamically allocate resources in both DL and UL, the scheduler can provide superior QoS for both DL and UL traffic.

### 3.2.2 Scheduler description

To efficiently support all types of connections (UGS, rtPS, ertPS, nrtPS and BE) as they are provided by the standard, the scheduler designed for PHYDYAS is based on ideas found in [21] and uses a combination of strict priority service discipline, earliest deadline first (EDF) [22] and weight fair queue (WFQ) [23] algorithms. The hierarchical structure of the bandwidth allocation is shown in Fig. 3.5. The bandwidth allocation per traffic class follows strict priority, from highest to lowest: UGS, ertPS, rtPS, nrtPS and BE. Within UGS connections fixed bandwidth allocation take place according to bandwidth requirements. Within ertPS and rtPS connections the earliest deadline first (EDF) bandwidth allocation is adopted while within nrtPS connections the weighted fair queue (WFQ) service is applied. Finally for BE connections the remaining bandwidth is equally allocated following the Round Robin model.

The scheduler combines both simplicity and efficiency, as can be easily implemented without the need for complex calculations, while it can provide service differentiation and QoS guarantees to all traffic classes. Simplicity is a critical requirement, as the algorithm has to operate in real-time on a frame-by-frame basis. Nevertheless, it is expected that this

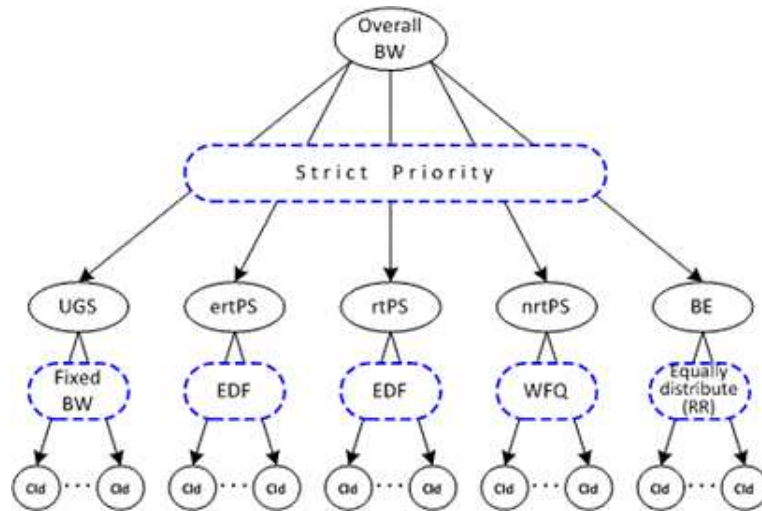


Figure 3.5: Representation of the scheduler's operation

will not sacrifice the algorithm's capability of operate under different traffic and channel conditions. Moreover, the scheduler can take advantage of the improved performance of filter bank based multicarrier (FBMC) system compared to cyclic prefix based OFDM (CP-OFDM) system, by fairly supporting a larger number of connections.

The proposed algorithm is described by the following rules:

1. *Overall data rate allocation:* The data rate allocation per traffic class follows strict priority, from highest to lowest: UGS, ertPS, rtPS, nrtPS and BE. One disadvantage of the strict priority service is that higher priority connections may lead lower priority connections to data rate starvation. To overcome this problem, a traffic policing module is included in each terminal, which forces the connections' data rate demands to stay within the traffic contract, as agreed during connection setup. This prevents the higher priority connections from using data rates more than their allocation, and allows for fair treatment of all traffic.
2. *Data rate allocation for UGS connections:* The scheduler allocates fixed data rates to UGS connections based on their fixed requirements. This policy is determined clearly by the IEEE 802.16 standard, without the need for real-time transmission requests.
3. *rate allocation for ertPS and rtPS connections:* The EDF service is adopted for these connections, to allow packets with the earliest deadline to be scheduled first. In case two packets belonging to two different service types (one of ertPS and one of rtPS) expire at exactly the same time, the scheduler will give priority to the ertPS packet, considering this packet of higher priority. Data rate needs are constantly updated through real-time transmission requests.
4. *Data rate allocation for nrtPS connections:* The weighted fair queue (WFQ) service

is applied for this traffic class. For each nrtPS connection, the ratio of its average data to the total nrtPS average data rates is computed, and resources being left from the higher priority classes (UGS,ertPS and rtPS) are distributed according to the computed weights of the connections. No transmission requests are required on this case.

5. *Data rate allocation for BE connections:* The remaining resources are equally allocated among BE connections following the Round Robin model, without transmission requests.

The scheduler described above was simulated emphasizing in the comparison between FBMC and CP-OFDM systems. Simulation parameters used in the RA is the same as those listed in [18].

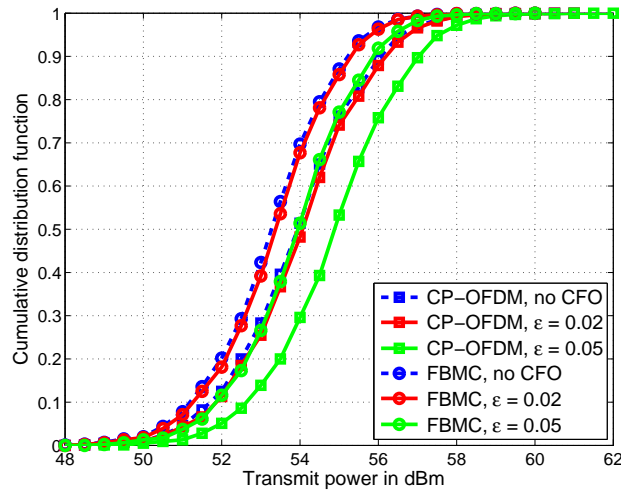
Firstly, to test the RA and compare the performances of CP-OFDM and FBMC systems, we design two lists of packets, one list of 40 small packets and the other of 20 larger packets with details given in Tab. 3.6, and use them as input to the RA. We assume that each packet comes from a different user, where the users are uniformly located in a cell of radius 2 km. The case that there are users with more than one packet to transmit can be easily accommodated.

Table 3.6: List of small and large packets

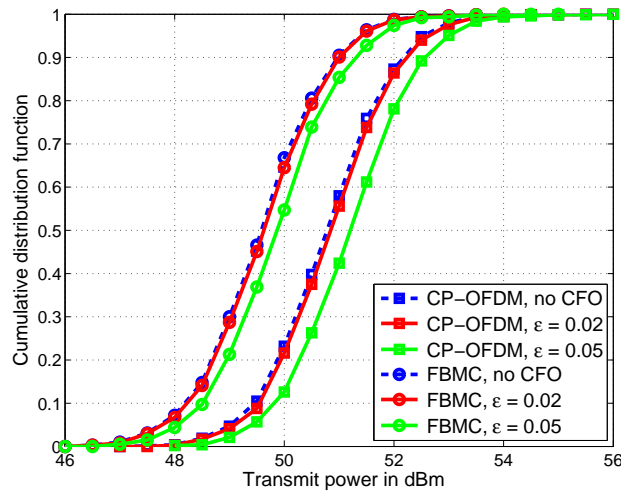
Packet $k$	$b_k$ / bytes	$\tau_k^{(\text{rq})}$ / ms	Packet $k$	$b_k$ / bytes	$\tau_k^{(\text{rq})}$ / ms
1 – 20	64	20	1 – 10	128	20
21 – 40	128	40	11 – 20	384	40

The two figures in Fig. 3.6 show the cumulative distributions of the minimum transmit power required in CP-OFDM and FBMC systems to serve the lists of large and small packets respectively, where two maximum residual CFO values  $\varepsilon = 0.02$  and  $\varepsilon = 0.05$  have been tested and the curves with no residual CFO are also drawn as a reference. On average, for the list of small packets, the FBMC system requires around 1.2 dBm less transmit power than the CP-OFDM system in the perfectly synchronized case, whereas for the list of large packets, the difference is 0.65 dBm. To compensate for the two residual CFO, the CP-OFDM system requires 0.0649 dBm and 0.4207 dBm more transmit power for the list of small packets, 0.1282 dBm and 0.9615 dBm more for the list of large packets, while the FBMC system requires 0.0427 dBm and 0.2863 dBm more transmit power for the list of small packets, 0.0903 dBm and 0.6576 dBm more for the list of large packets, respectively. This demonstrates from a QoS provisioning and resource allocation point of view, that the FBMC system is less sensitive to CFO and benefits more from multiuser diversity, and its advantage is even larger when the CFO or the number of packets increases.

To reveal the effectiveness of the proposed scheduling and resource allocation procedure in terms of differentiated QoS, we execute a scenario involving an increasing number of users, each one with one active connection per service type. Fig. 3.7 shows the input and



(a) With the list of large packets



(b) With the list of small packets

Figure 3.6: CDF of minimum transmit power in CP-OFDM and FBMC systems with different residual CFO

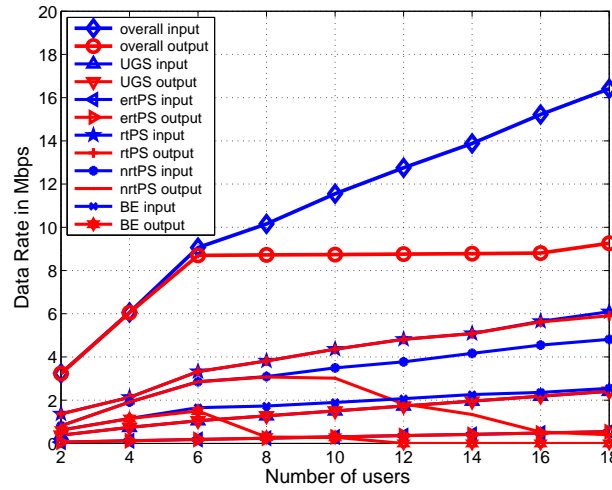


Figure 3.7: CP-OFDM input and output data rates

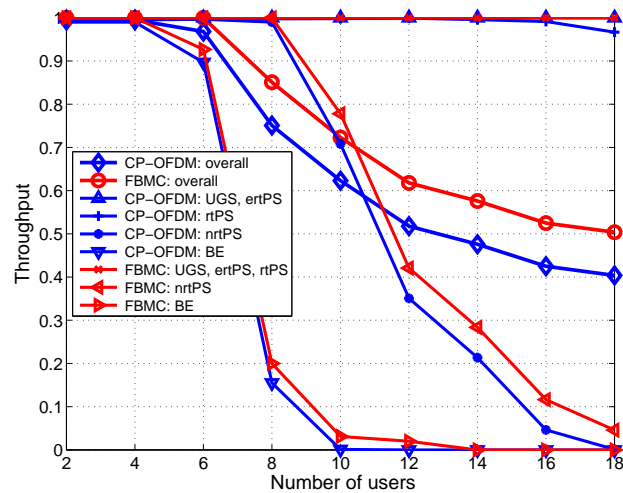


Figure 3.8: Throughput in CP-OFDM and FBMC systems

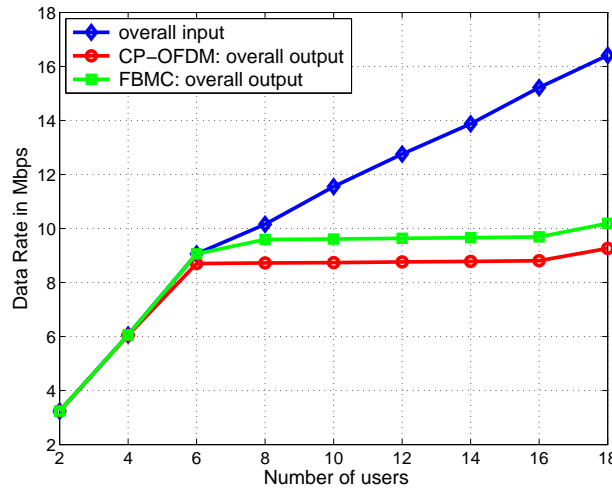


Figure 3.9: Input and output data rates in CP-OFDM and FBMC systems

output data rates in the system for the CP-OFDM case. For up to 6 users, the system manages to service all incoming traffic with no losses. After this point, BE, that is the type with the lower priority, starts facing denial of service, to allow transmission of higher priority traffic. As the load increases, nrtPS output data rate is reduced (after 8 users), leaving most of the capacity for the real-time service types. At the end of the simulation (18 users), the load is increased up to a point that even rtPS traffic starts facing losses. Fig. 3.8 shows the attained throughput per service type as a percentage of the offered traffic for both CP-OFDM and FBMC. Again, the differentiated treatment is clearly revealed forcing BE connections to reduce their throughput first, followed by nrtPS and rtPS. An overall throughput improvement of approximately up to 18% is attained with FBMC, compared to CP-OFDM, as a result of the improved operation of the physical layer. Finally, the comparative performance of FBMC and CP-OFDM in terms of overall data rates is shown in Fig. 3.9. The effectiveness of FBMC is indicated by an almost stable increase of the data rate for most of the cases.

### 3.3 Cross-Layer scheduling methods

The efficient support of a wide set of network applications under a variety of conditions is considered as one of the most important requirements for modern wireless communication systems. To address this complex issue, different performance improvement mechanisms are introduced in almost all layers of a typical wireless protocol stack. Such mechanisms include the multi-encoding rate functionality at the Application layer, the adaptive Automatic Repeat Request (ARQ) mechanisms at the Transport layer, the adaptive routing at the Network layer, the adaptive Forward Error Correction (FEC) and appropriate resource allocation at the Medium Access Control (MAC) layer, and the adaptive modulation,



coding and power control mechanisms at the Physical (PHY) layer. Although these mechanisms have been initially designed to work independently, there is an increasing need for the development of a scheme that will allow for their efficient cooperation towards optimized system performance. This need emerges from the fact that their independent parallel operation may result in inefficiencies caused mainly by possible conflicting actions.

In the recent bibliography we can find a great variety of proposals on cross-layer schemes designed for numerous kinds of wireless networks and applications. In the following cross-layer schemes focusing on Quality of Service (QoS) and throughput improvement and Radio Resource Management (RRM) for real-time traffic are presented while in next subsection a cross-layer mechanism over real time traffic for WiMAX networks is described.

### 3.3.1 Cross-layer schemes in the bibliography

A large number of recent proposals on cross-layer design aim at improving the QoS provision and the overall performance of the system they are applied to. Such proposals include rate control algorithms based on the experienced channel conditions that aim to normalize the unpleasant variations of the wireless medium quality. Other mechanisms introduce efficient schemes to avoid unnecessary retransmissions and improve the system throughput. Adaptive coding schemes that take into account both the QoS requirements of the applications and the conditions of the wireless medium are also suggested [24, 25, 26]. Many other proposals focus on QoS support in multimedia applications while the majority of them deal with the support of demanding multimedia applications [27, 28, 29, 30, 31].

The air interface and hardware resources need to be efficiently utilized to achieve increased throughput and channel capacity and avoid unpleasant phenomena such as interference. Several proposals on crosslayer designs regarding RRM can be found in the recent bibliography. The majority of them introduce efficient schemes for power control, resource allocation, admission control and packet scheduling [32, 33, 34, 35].

### 3.3.2 The cross-layer optimization mechanism

The cross-layer mechanism for real-time traffic over WiMAX networks described here is based on the architectural framework introduced in [31], which consists of N layers and a cross-layer optimizer. According to this framework, the optimization process is performed in three steps:

1. *Layer abstraction*: Computes an abstraction of layer-specific parameters that are processed by the optimizer. This process aims at reducing the overall data processing and communication overhead while maintaining consistency.
2. *Optimization*: Determines the values of layer parameters that optimize a specific objective function.

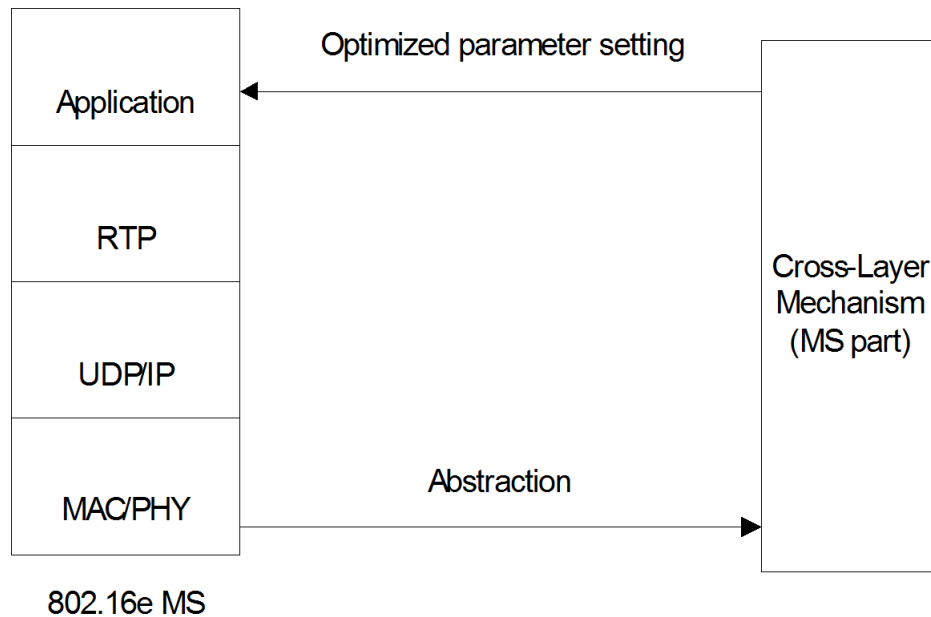


Figure 3.10: BS (a) and MS (b) part functionality

3. *Layer reconfiguration*: Distributes the optimal values of the abstracted parameters to the corresponding layers that in turn translate them back into layer-specific information.

The mechanism described in this section works in three layers, namely the Physical, Data-Link (MAC) and Application layers. The cross-layer mechanism for WiMax networks is split into two parts, namely the Base Station (BS) part and the Mobile Station (MS) part, residing at the BS and the MSs of a WiMax network respectively (Fig. 3.10). The BS part accepts an abstraction of layer-specific information, namely, the channel conditions, QoS parameters and transmission power capabilities of all active connections, provided by the BS PHY and MAC layers (Step 1: Layer Abstraction). According to this information, a decision algorithm determines the desired encoding mode of each MS, separately for each direction (uplink or downlink) (Step 2: Optimization). Finally, the BS part configures the corresponding layers with the determined parameters (Step 3: Layer Reconfiguration) (Fig. 3.10 (a)). The MS part may either accept the BS part's suggestions regarding encoding mode adjustments or refine them, based on its better knowledge of the status of the MS's active connections and instruct the MS application layer accordingly (Fig. 3.10 (b)).

The operation of the cross-layer mechanism for both uplink and downlink directions can be divided in three main phases:

- In Phase 1, the BS part starts by collecting all the required information regarding the performance status of each of its active connections. This information includes

channel state conditions on the uplink and downlink directions, packet timeout rate and mean delay.

- In Phase 2, the BS part uses the collected information to run a decision algorithm and decide on the Application layer encoding mode used. This decision is taken separately for each MS aiming at providing an improved QoS.
- In Phase 3, the BS MAC layer transfers to the MS MAC layer its decisions about encoding mode adjustments. These decisions are transferred using the Rate Adjustment Request (RATE-ADJ-REQ) message defined in [11]. The MS MAC layer transfers the received rate modification request to the MS part that in turn decides on the connections that should be affected and sends proper cross-layer messages to the Application layer.

### 3.3.3 Decision algorithm

Focusing on the second phase of the cross-layer mechanism described above a decision algorithm is proposed that takes into account the packet loss rates and mean delay of each connection and decides on the adaptation of the encoding mode at the Application layer. The actions to be taken by the decision algorithm are as follows (Fig. 3.11):

1. In case the Packet Loss Rate (PLR) exceeds the connections maximum PLR threshold, referred to as  $PLR_{th_{high}}$  ( $PLR > PLR_{th_{high}}$ ) the connection is suffering from increased packet loss that significantly deteriorates its QoS. In that case, the BS part decides to set the Application layer encoding mode to its minimum value in order to moderate timeouts and reduce packet losses.
2. In case the mean delay exceeds the connection delay bound, referred to as  $delay_{th_{high}}$ , ( $delay > delay_{th_{high}}$ ) the connection is considered to be facing increasing mean delay that may result in packet timeouts. In order to avoid further delay increase and packet timeouts, the decision algorithm instructs for an encoding rate decrease that will reduce the experienced delay.

Respectively, when the loss rate and the mean delay decrease significantly, ( $PLR < PLR_{th_{low}}$  and  $delay < delay_{th_{low}}$ ), the BS part may instructs for an encoding rate increase to improve the QoS provided to the user.

It is worth noting that the performance of such a decision algorithm depends much on the selected delay and loss thresholds, as these can make the operation too sensitive (initiating changing of encodings rates too often), or too insensitive (not initiating changing of encoding rates when needed). As the channel and traffic condition are dynamic, an adaptable thresholds setting would be required for optimal performance.

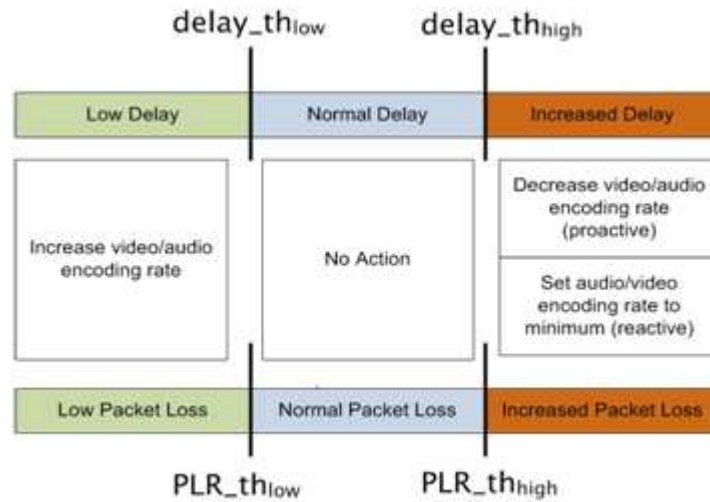


Figure 3.11: Decision algorithm scheme

### 3.3.4 Simulation model and results

The decision algorithm described above was implemented with Matlab 7.6 under the simulation model depicted in Figure 3.12. As it can be seen, the model consists of a number of components, each one implemented as a Matlab object, interconnected to each other.

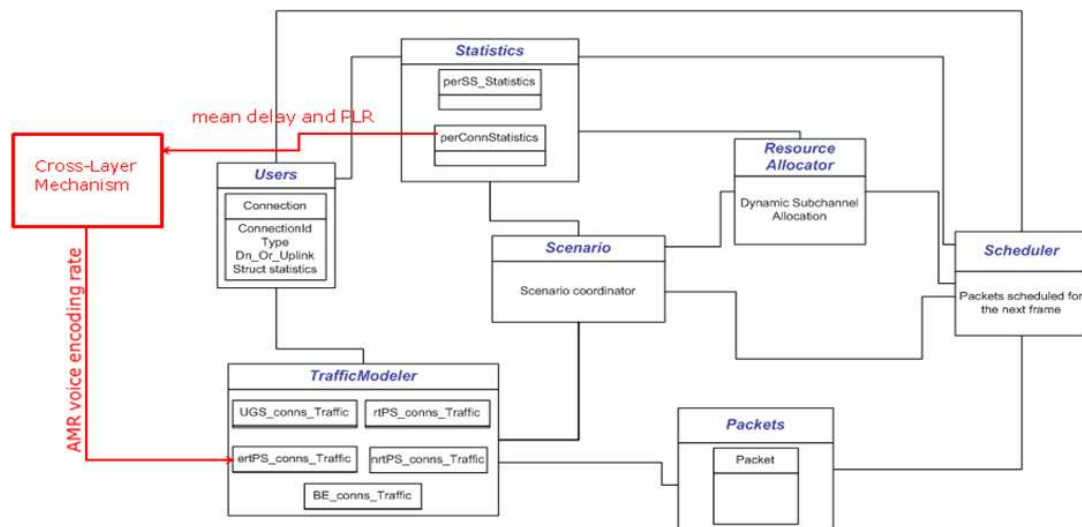


Figure 3.12: Simulation model

Cross-layering is implemented in order to adjust the encoding rate of voice traffic based on the performance metrics of the MAC layer. The “Cross-Layer Mechanism” object gets

the mean delay and packet loss rate information from the “Statistics” object, executes the decision algorithm, and, based on its outcome, communicates with the “TrafficModeller” to provide the new AMR (Adaptive Multi Rate) voice encoding rate. Since voice is using the ertPS traffic class of WiMAX, only this traffic generator affected. Finally, the “Packets” object contains an ordered list of objects of type “Packet”, that hold all the information related to the packets inside the system, at any instance of time. This is the reason of placing “Packets” object in the middle of the above figure, as it is not a functional model like e.g. the RA object. The simulation parameters are summarized in Table 3.7. Focusing on ErtPS service type the packet mean delay and the packet loss rate were calculated for variable number of users in the system.

Traffic model	
Number of users	Variable from 20 to 170
Connections per user	1
service types	UGS, ErtPS,rtPS,nrtPS,BE
Percentage of ErtPS connections (%)	30%
Frame duration (ms)	5 (ms)
Thresholds	
Delay high threshold (ms)	20
Delay low threshold (ms)	12
PLR high threshold (%)	10%
PLR low threshold (%)	5%
Number of Video/Audio encoding rates	8

Table 3.7: Simulation parameters

Figure 3.13 depicts the improvement of ErtPs packets mean delay under the proposed cross layer mechanism’s control. The mechanism activated when the mean delay is below the low threshold or exceeds the high threshold. In case that the mean delay exceed the high threshold, the decision algorithm that used by the mechanism instructs for an encoding rate decrease leading to 25%-30% reduce of the mean delay. In case that the mean delay is below the low threshold, the action of the proposed mechanism leading to slight increase of the delay, however allows for further improve of the QoS provided to the user. It is also mentioned that the mean delay (with or without the mechanism) increases faster when the number of users exceeds 110 due to the effect of the system’s capacity limitation.

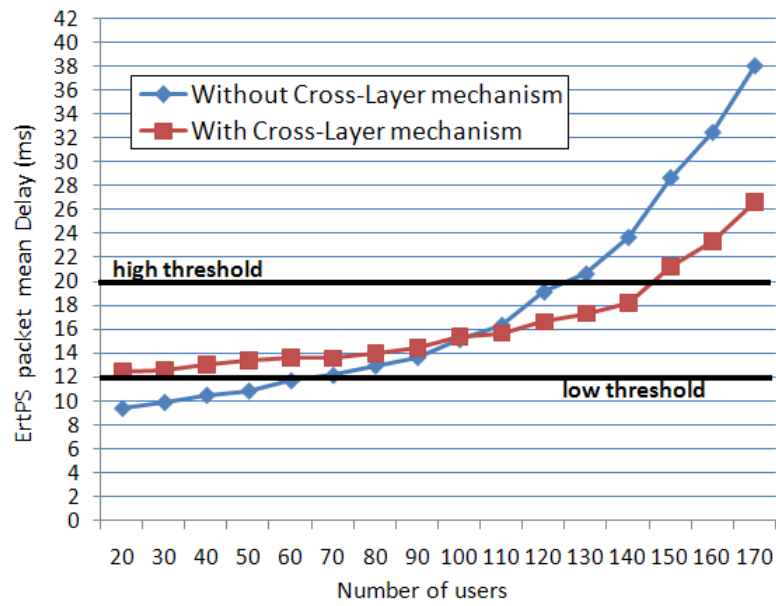


Figure 3.13: Mean delay for ErtPS packets.

Figure 3.14 shows the improvement of ErtPs packets loss under the proposed cross layer mechanism's control. The mechanism activated when the percentage of loss ErtPS packets is below the low threshold or exceeds the high threshold. In case the packet loss exceeds the  $PLR_{th_{high}}$ , the BS part of the mechanism decides to set the Application layer encoding mode to its minimum value improving the percentage of ErtPS loss packets from 20% to 35%. In contrast with the delay improvement the decision of immediate minimizing the application layer encoding, than just decrease it, when the PLR exceed the high threshold, directly effect the PLR value explaining the sharp changing in red curve when it crosses the high threshold line in Figure 3.14 (from 110 users to 120 users).

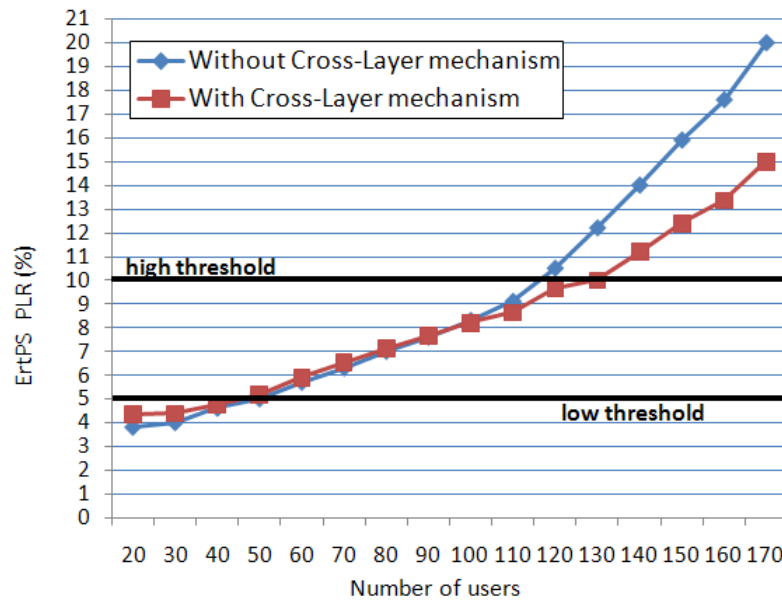


Figure 3.14: ErtPS packet loss.

### 3.4 Simulation results for the joint scheduling and resource allocation approach

In addition to the proportional fair scheduler (PFS) and in order to validate and to check the performance of the proposed Time Stamped Packets Scheduling (TSPS) scheduling jointly with a modified version of the PFS named Buffer Based PFS (b<sup>2</sup>PFS)<sup>1</sup> scheme in Deliverable [10] and in [18] were evaluated, where, instead of balancing the throughput of the different users the proposed scheduler equalizes the number of buffered bits from each user, therefore the variable bit rate (VBR) streams can be managed.

First, the performance of the proposed TSPS prioritization function was evaluated and compared to the PFS and the b<sup>2</sup>PFS. The allocation algorithm follows the one proposed in [10]. For the PFS and b<sup>2</sup>PFS scheduling functions, the number of bits per frame  $b_i$  that should be transmitted is assumed equal to the number of buffered bits ( $b_i = L_i(t)$ ). The latency scale is fixed to 10 frames (i.e.  $\alpha = 10$ ).

The metric of packet delay statistics given by different scheduling algorithms for *nrtPS* traffic case are presented in Fig. 3.15, where the assumed number of active MSs within the cell is  $K = 15$ . The traffic from all the users is modelled according to [36] with a VBR streams with an average data rate of 2Mbps. Thus an average system throughput of 30Mbps is required. The maximum delay per packet is assumed 300ms. The main

<sup>1</sup>The prioritization function of the b<sup>2</sup>PFS scheduler was detailed in subsection 4.3.2.4 of deliverable D6.1 [10].

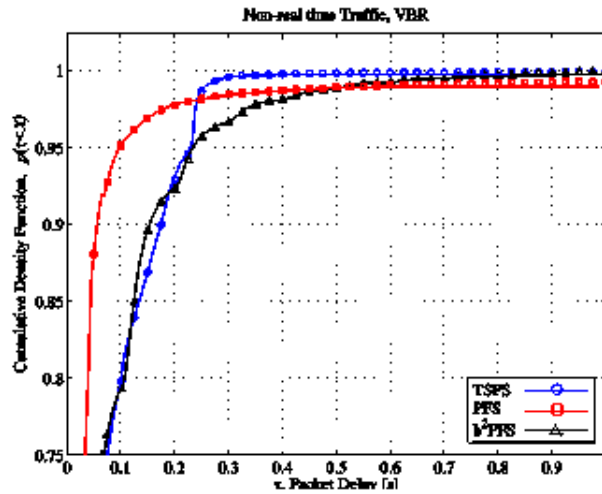


Figure 3.15: Cumulative density function of the packet delay for non-real time traffic and  $K = 15$  users

observations are:

- The 99th percentile of each prioritization function is 275ms for TSPS, 535ms for PFS, and 530ms for the b<sup>2</sup>PFS.
- The appreciated improvement in TSPS scheduler is mainly due the effect of the urgency factor ( $P_{urgency}$ ), since the slope of the cumulative density function (cdf) is changed for delays higher than the value  $\tau_{max} - \Delta\tau$ , where the guard time was fixed to  $\Delta\tau = 0.2 \times \tau_{max}$ .
- The maximum delay achieved by the “b<sup>2</sup>PFS” scheduler is much lower than that with PFS. This is mainly due the fact that the b<sup>2</sup>PFS considers each time the actual state of the buffers.
- Thus when a large packet is received the related assigned queue priority is increased, whereas the PFS scheduler is optimized to balance the throughput from all the users during short periods.

Using the same number of active users and the same average bit rate per user of 2Mbps, we have observed that with CBR traffic, the 99th percentile is reached at 55ms, 100ms and 125ms for the TSPS, PFS and b<sup>2</sup>PFS schedulers respectively. As expected, better performances are achieved having VBR traffic. However, only the TSPS and the “b<sup>2</sup>PFS” were able to send all the packets within the maximum packet delay for the CBR traffic.

In case of rtPS traffic, having a packet not transmitted within the maximum delay, the packet is deleted from the queue and discarded. Fig. 3.16 shows the cdf of the packet delay for this scenario having 50 and 100 users. As it is shown, for  $K = 50$  all the methods



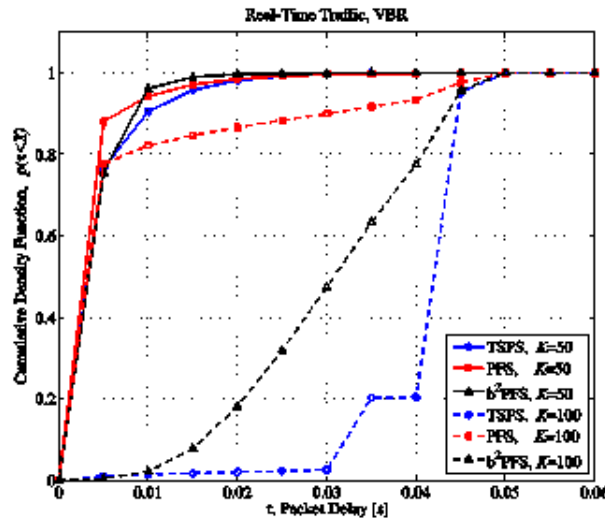


Figure 3.16: Cumulative density function of the packet delay for real time traffic and  $K = \{50, 100\}$  users

achieve a delay lower than the maximum allowed (50ms), in fact the 99th percentile of the managed delay is 25ms for TSPS and PFS, and 15ms for the  $b^2$ PFS. Furthermore, the packet loss rate for each scheme is 0% for the TSPS,  $1.6 \cdot 10^{-3}\%$  for the PFS and  $1.6 \cdot 10^{-4}\%$  for the  $b^2$ PFS. In case  $K = 100$ , it can be observed that the PFS is the only one that achieves lower packet delays, and that the TSPS sent most of the packets when the urgency factor is applied (the urgency factor is here applied when  $\tau \geq \tau_{\max} - \Delta\tau = 0.04s$ ). For  $K = 100$ , the packet loss rate for each scheduling function is 8.98%, 33.4% and 16.97% for the TSPS, the PFS, and the  $b^2$ PFS respectively. Note that for the TSPS although most of the packets are sent when they are nearly to expire, it achieves a lower packet loss rate.

- So, despite the TSPS initially implies an increase on the computational complexity since it requires more information about the buffers status (i.e. each packet must be time stamped for the TSPS scheduler), its superiority has been shown for real time and non-real time applications. Moreover, there is no necessity to update the priorities each time a MRU is allocated, thus the computational complexity is also drastically reduced compared to the PFS and the  $b^2$ PFS.
- Each traffic type achieves a maximum packet delay lower than the maximum tolerated.
- Another advantage of the proposed TSPS scheduler is that it can easily manage different traffic types by applying different maximum delays to each stream.

Analysing the performance of the TSPS scheduler in heterogeneous traffic, Fig. 3.17 shown the density function of the packet delay when mixed traffic services are used in the

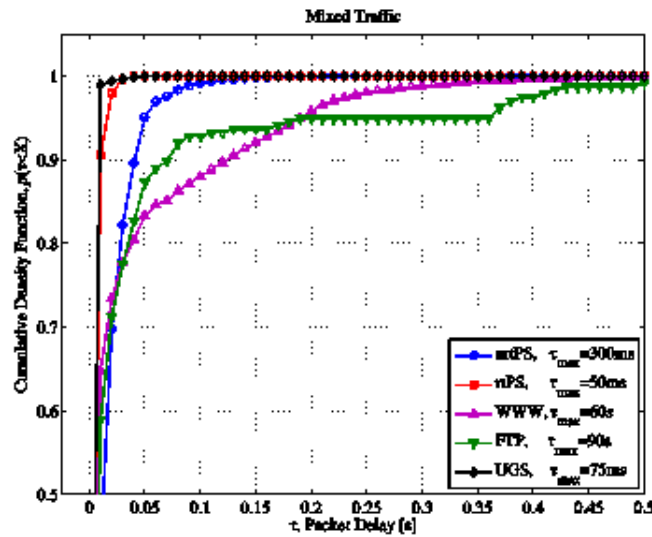


Figure 3.17: Cumulative density function of the packet delay for mixed traffic obtained with the TSPS scheduling function and  $K = 50$  users

network. The evaluation was tackled using  $K = 50$  active users, 10 of them have *nrtPS* service applications, 13 users require *rtPS* applications, 10 users are browsing internet files (World Wide Web - *www*- service), 5 users are downloading files according with the File Transfer Protocol (FTP), and finally 12 users demand UGS connections. The total measured downlink throughput is 26.54Mbps, and the maximum delay for each service is based on the parameter depicted in Table 4.4 in [10]. For “*www*” and the FTP services, despite there is no delay restrictions (i.e.  $\tau_{\max} = \infty$ ), a maximum delay of  $\tau_{\max} = 60s$  and  $\tau_{\max} = 90s$  has been assumed for both services respectively. Using the above scenario and assumptions, the main observed behaviours are:

- The 99th percentile for the delay sensitive applications is at 95ms, 25ms and 15ms for the *nrtPS*, the *rtPS* and the UGS respectively.
- The UGS service application achieves lower delay than that obtained for *rtPS* despite having a higher packet delay value.

This latter behaviour could be justified by the fact that the UGS’s packet services are much smaller than those from the *rtPS* applications. Thus, fragmentation is not applied in most cases.

Having illustrated the performance of the proposed TSPS prioritization function, the next figures depict the performance analysis of the proposed resource allocation algorithm in Figure 4.9 of [10]. The statistics related with the number of bursts per frame by using proposed algorithm are shown in Fig. 3.18. Here, the analysed scenario is constituted by a total of  $K = 15$  active users, each one requiring *nrtPS* services. The number of required bursts per frame is analyzed as a function of the  $P_{\text{burst}}$  factor having the following values

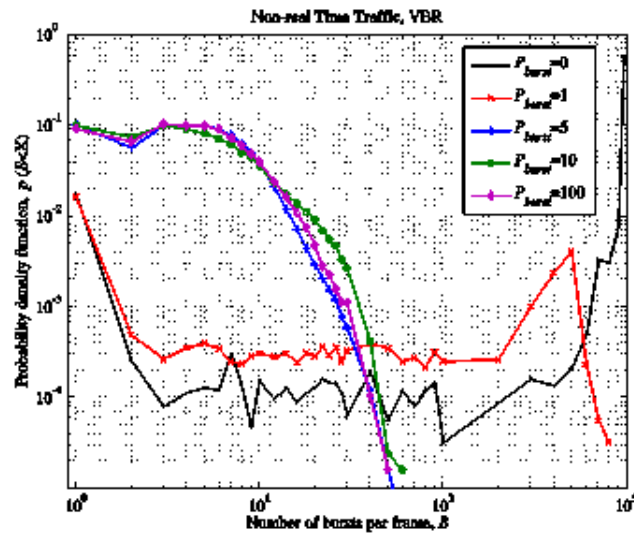


Figure 3.18: density function of the number of bursts per frame for *nrtPS*,  $K = 15$  users and different values of the  $P_{\text{burst}}$  factor (when the TSPS prioritization function is applied)

$P_{\text{burst}} = \{0, 1, 5, 10, 100\}$ . The prioritization function within the proposed TSPS is here applied (see equations in section 4.3.1.2 of [10]). In case  $P_{\text{burst}} = 0$ , the algorithm considers that each new allocated MRU is a new burst. Thus this is the maximum granularity case, but clearly in this extreme case the signalling is unaffordable. After running simulations, the main obtained observations are:

- for  $P_{\text{burst}} > 0$ , the algorithm starts to merge the MRUs into bursts. For  $P_{\text{burst}} = 1$ , during the allocation of each MRU, half of them are allocated to an existing burst. Hence, the number of bursts for  $P_{\text{burst}} = 1$  is still unaffordable in terms of required signalling.
- for  $P_{\text{burst}} \geq 5$  it is observed that the number of bursts is lower than 60 for all the simulated frames. Furthermore, in case  $P_{\text{burst}} = 5$ , the achieved number of bursts per frame is lower than 24 in 99% of the transmitted frames, which can be considered as a very encouraging result. Assuming approximately 60 bits are required for signalling for each burst [37], having a QPSK modulation and a code rate 1/3, the downlink signalling zone (i.e. the DL-MAP) would span less than 2 symbols which means that the loss due to the downlink signalling is 6.66% for the downlink mode when having a total of 60 FBMC symbols (which is equivalent to 30 OFDM symbols) per subframe.

On the other hand, the obtained efficiency by the proposed described algorithm in Figure 4.9 of subsection 4.3.2.4 in [10] is depicted in Fig. 3.19 as a function of the  $P_{\text{burst}}$  factor. The simulated scenario is exactly the same as in Fig. 3.18.

- It is clear that as  $P_{\text{burst}}$  increases the spectral efficiency decreases. In case  $P_{\text{burst}} = 0$ , two main behaviours are observed. First, almost the frames sent with a very

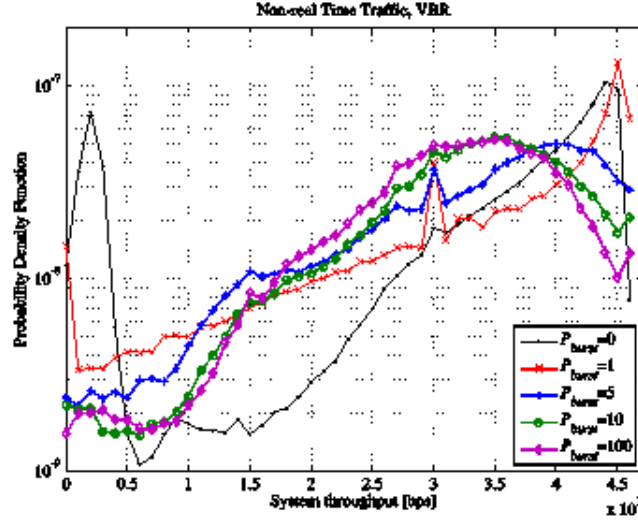


Figure 3.19: Probability density function of the system throughput for *nrtPS*,  $K = 15$  users and different values of the  $P_{\text{burst}}$  factor (when the TSPS prioritization function is applied)

high spectral efficiency achieves the maximum throughput which is approximately 46Mbps, however it can be observed that many frames have been sent quite unfilled due to the lack of buffered bits leading to a low system throughput (peak on the left side of the figure).

- ” When we compute the 99th percentile of the packet delay for each  $P_{\text{burst}}$  value, the following delay values have been obtained  $\{160, 185, 250, 275, 725\}$  [ms] for  $P_{\text{burst}} = \{0, 1, 5, 10, 100\}$  respectively.

Analysing and comparing these latter results with those obtain in Fig. 3.17, it can be concluded that having  $P_{\text{burst}} = 5$  offers the best trade off between granularity (i.e. spectral efficiency), required signalling, and QoS requirements.

In order to evaluate the performance of the JRAS-RDP algorithm with limited feedback the system described in Section 4.3.3.1 of deliverable [18] have been used. The shape of the RUs for the localized bursts is  $N_{\text{sc}} = 18$  and  $N_{\text{sd}} = 3$ , whereas the distributed burst are formed by 6 tiles (i.e.  $N_t = 6$ ) with 3 sub-carriers and 3 symbols each tile (i.e.  $N_{\text{st}} = 9$ ). The loss due to pilot subcarriers in both types of RUs is a function of the pilot density  $\mu_p = 8/9$ . We have assumed that the Mixed and Band AMC (MTBA) zone (see algorithm flow chart in Figure 4.12 in deliverable D6.1 in [10]) spans over the whole useful downlink subframe hence  $N_S = 43$  FBMC symbols (equivalent of 30 symbols in OFDM system). The performance of the proposal is assessed only for Best Effort (BE) traffic by varying the number of active users  $K$ , and knowledge values of the CSI at the BS. The main evaluated performances are the spectral efficiency in order to observe the effects of

signalling reduction, and the packet delay to determine if the system is able to guarantee the different QoS requirements.

In order to take into account the loss due to the signalling (channel feedback and DL-MAP transmission), we used equation (4.31) in deliverable [18] to calculate the system spectral efficiency “ $\nu$ ”. Equation (4.31) in [18] depends mainly from: i) the data bits transmitted at a burst  $d$ , ii) the spectral efficiency of the MCS applied to the proper burst, and iii) finally the total number of transmitted bursts during the whole simulation time. “ $\nu$ ” depends also of  $B_{\text{CSI}}$  and  $B_{\text{SNR}}$  which are the bits transmitted by MSs in the uplink to report the CSI of their  $n$ -best subchannels, and the average SNR respectively.

During the simulations It was considered that the signalling bits are transmitted with a BPSK and a coding rate  $1/2$ , thus the term  $r_{\text{sign}}$  (means the spectral efficiency of the MCS used to transmit the signalling) which means that the spectral efficiency of the MCS used to transmit the signalling is equal to  $r_{\text{sign}} = 0.5$ .

The amount bits of signalling required for each burst is 60 and 43 the each localized and distributed burst respectively. Since the bits for signalling are transmitted following the PUSC SNR thresholds [37] being sure that these bits are properly decoded ( $\text{BER} < 10^{-6}$ ) for any user within a range of 1.69 km. Consequently, the users at the cell border are able to decode properly the DL-MAP. On the other hand, to obtain the term  $B_{\text{CSI}}$  we have considered that the MS feedback the SNR value of their  $n$ -best subchannels with 6 bits, thus the SNR range of 0-32dB is sampled with steps of 0.5 dB. Likewise, the average SNR is fed back from all the MSs every 15ms with a codeword of 6 bits length.

In the first scenario,  $K$  different active users ( $K = \{25, 50, 75, 100, 125, 150\}$ ) are evaluated where each user’s service flow is simulated under the *web browsing test service*. For this service class, the packet delay is unrestricted and the maximum BER for this service class is equal to  $10^{-6}$ . The traffic is modelled such that a web browsing session is simulated. The reading time between two consecutive packet calls has been reduced to 20s to increase the link activity. A simulation time  $T_{\text{sim}} = 125\text{s}$  has been used for this scenario in order to include different packets calls. Fig. 3.20, depicts obtained results based on above scenario, and the main observations are:

- For the continuous feedback case, the spectral efficiency is highly reduced as  $n$  is increased leading to a (nearly) zero spectral efficiency for the Full-CSI knowledge case. Ones can conclude that when the MS have to report their channel independently from the input buffers, the gain due to multiuser diversity is neutralized by the loss caused by the uplink signalling.
- For the BS requested feedback case, we observed a slight increase of the spectral efficiency as  $n$  is increased. This shows that as the knowledge of the channel is improved, the spectral efficiency can be increased if the AMC is applied.
- Since the traffic simulated is bursty type, we have observed that the number of the MSs that need to be served simultaneously is on average between 1 and 4 for  $K = 25$  and  $K = 150$  respectively. Clearly, in this case the gain due to multiuser diversity is quite limited as consequence of the bursty nature of the traffic. Larger gains and

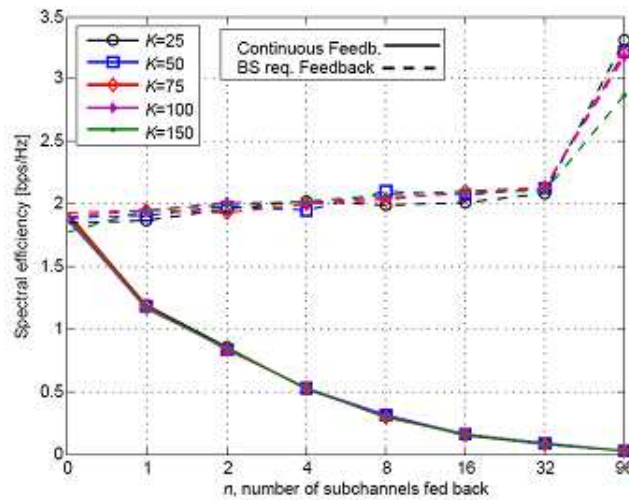


Figure 3.20: Spectral efficiency performance using the JRAS-RDP with limited feedback algorithm and the MTBA zone as a function of the number of subchannels fed back  $n$  and the number of users  $K$

spectral efficiencies could be expected for real-time and non-real time traffic where the number of simultaneously active users is much higher.

Regarding the 99th percentile of the packets delay (Fig. 3.21) the main conclusions are:

- By combining distributed and localized bursts, the delay can be reduced more than one order of magnitude. If we compare the delay in case there is no CSI at the transmitter (i.e.  $n = 0$ ) to the  $n = 1$  case, the difference in delay between both schemes is very noticeable (more than one order of magnitude for  $K > 50$ ). This is due to the fact that since the localized bursts have been prioritized over the distributed bursts, it is more than probable that every user is allocated one low rate data channel which guarantees the minimum throughput
- It was also observed that if  $n$  is increase, this minimum throughput increase and a reduction on the packet delay is achieved.
- For values of  $n > 4$  a very slight improvements are achieved

The amount of resources required for downlink and uplink signalling (DL-MAP length and n-best subchannels feedback load) is also analyzed. Fig. 3.22 shows the sum of downlink and uplink signalling in terms of number of required OFDM symbols per frame. To obtain the number of FBMC symbols occupied by the signalling we have considered that all the signalling (downlink and uplink) is transmitted with a BPSK modulation and a coding rate equal to  $1/2$ . Therefore, the number of signalling bits that can be fitted within one/two OFDM/FBMC symbol (with 1728 active subcarriers) is 768 bits (i.e.  $1728 \times 1/2 \times \mu_p = 768$ ). The main achieved results are:

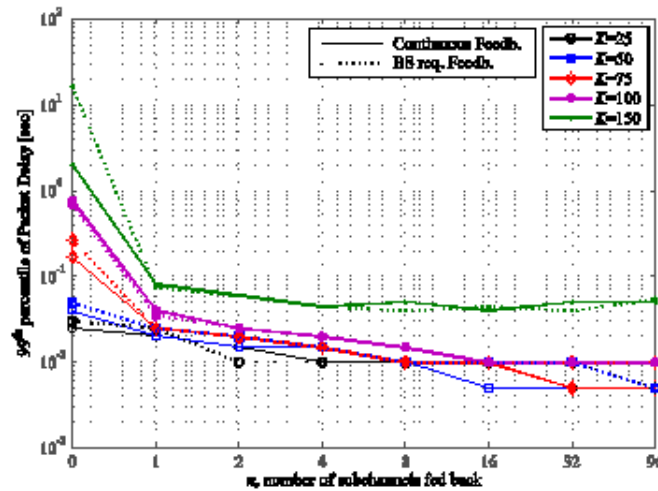


Figure 3.21: 99th percentile evaluation of the packet delay as a function of  $n$  and  $K$

- $K$  or  $n$  are increased the amount of signalling is increased. If we assume that 10 FBMC symbols (which is equivalent to five OFDM symbols) can be dedicated to signalling within one frame. We can conclude that the best combination pairs of  $\{K, n\}$  are  $\{50, 8\}$ ,  $\{100, 4\}$ , and  $\{150, 2\}$ . As a result, by modifying  $n$  a trade-off between the required signalling and the system spectral efficiency (and delay) can be achieved.
- An interesting observed result was that the delay can be highly improved in case both *localized* and *distributed* bursts are combined. Really, the use of localized bursts guarantees that unless the system is very saturated every user will have at least one designed subchannel. This brings up the idea of adapting the number of feedback subchannel according to user requirements or certain fixed priorities.
- Using the MTBA zones, a tradeoff between spectral efficiency, delay and load signalling requirements could be achieved by optimizing the number of sub-channels signalled in the uplink.

Based on the above summarised results, it can be concluded that the JRAS-RDP with limited feedback algorithm and the MTBA can be also used in multiplexing. A distribution strategy could be to allocate users with low mobility in localized bursts, and those with high mobility in distributed bursts. This will allow to increase the transmit diversity and the spectral efficiency in high and low mobility users' scenarios respectively. The MTBA could here be considered as a tool to use the whole transmission frames more efficiently depending on the user's scenarios needs.

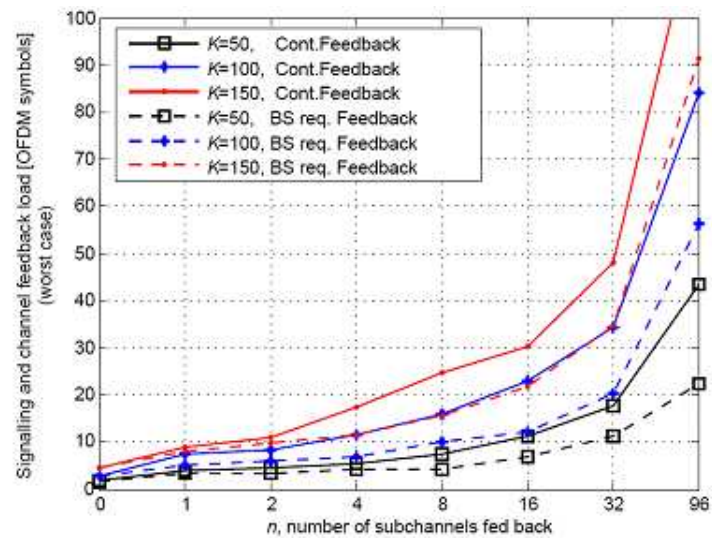


Figure 3.22: Total signalling requirements in the downlink and uplink as a function of  $n$  and  $K$



# Chapter 4

## Conclusions

Detailed conclusions have been provided at the end of the different sections. The following contributions of work package 6 are worth emphasizing:

- In multicell networks FBMC systems are not sensitive to inter-cell lack of synchronization due to the good frequency localization of the prototype filter. Intercell interference can be better coordinated in an FBMC system and will lead to more efficient frequency reuse in a cellular environment.
- Scheduling and resource allocation can benefit from the greater robustness with respect to synchronization errors and simpler interference coordination of FBMC in both uplink and downlink.



# Bibliography

- [1] S. N. Moiseev, S. A. Filin, M. S. Kondakov, A. V. Garmonov, D. H. Yim, and J. Lee, "Analysis of the statistical properties of the interference in the IEEE 802.16 OFDMA network," in *Proc. IEEE Wireless Communications and Networking Conference WCNC 2006*, vol. 4, 3–6 April 2006, pp. 1830–1835.
- [2] C. Huo, A. B. Sesay, and A. O. Fapojuwo, "Co-channel diversity schemes for an OFDM based cellular system with one-cell frequency reuse," in *Proc. IEEE Wireless Communications and Networking Conference WCNC 2006*, vol. 2, 3–6 April 2006, pp. 798–803.
- [3] J. Cheng and N. C. Beaulieu, "Accurate DS-CDMA bit-error probability calculation in rayleigh fading," *IEEE Trans. Wireless Commun.*, vol. 1, no. 1, pp. 3–15, 2002.
- [4] X. Wang, T. T. Tjhung, Y. Wu, and B. Caron, "SER performance evaluation and optimization of OFDM system with residual frequency and timing offsets from imperfect synchronization," *IEEE Trans. Broadcast.*, vol. 49, no. 2, pp. 170–177, 2003.
- [5] H. Zhang, D. L. Ruyet, D. Roviras, Y. Medjahdi, and H. Sun, "Spectral efficiency comparison of OFDM/FBMC for uplink cognitive radio networks," *EURASIP Journal on Advances in Signal Processing*, vol. 2010, p. 14 pages, 2010.
- [6] T. Weiss, J. Hillenbrand, A. Krohn, and F. K. Jondral, "Mutual interference in OFDM-based spectrum pooling systems," in *Proc. VTC 2004-Spring Vehicular Technology Conf. 2004 IEEE 59th*, vol. 4, 2004, pp. 1873–1877.
- [7] S. Y. Shin, H. S. Park, and W. H. Kwon, "Mutual interference analysis of IEEE 802.15.4 and IEEE 802.11b," *Computer Networks*, vol. 51, no. 12, pp. 3338 – 3353, 2007. [Online]. Available: <http://www.sciencedirect.com/science/article/B6VRG-4N146DX-1/2/9caff7db0f72d1365cb3de354864c128>
- [8] K. A. Hamdi and Y. M. Shobowale, "Interference analysis in downlink OFDM considering imperfect intercell synchronization," *IEEE Trans. Veh. Technol.*, vol. 58, no. 7, pp. 3283–3291, 2009.
- [9] Y. Medjahdi, M. Terre, D. Le Ruyet, D. Roviras, J. A. Nossek, and L. Baltar, "Inter-cell interference analysis for OFDM/FBMC systems," in *Proc. IEEE 10th Workshop*

- Signal Processing Advances in Wireless Communications SPAWC '09*, 2009, pp. 598–602.
- [10] European project ICT-211887 PHYDYAS, “Deliverable D6.1: Duplexing and multiple access techniques, software description,” <http://www.ict-phydyas.org>, Tech. Rep., January 2009.
  - [11] Y. Medjahdi, M. Terre, D. L. Ruyet, and D. Roviras, “A new model for interference analysis in asynchronous multi-carrier transmission,” 2010, submitted to *IEEE Trans. Wireless Communications*.
  - [12] M. Bellanger, “Filter banks and OFDM-OQAM for high throughput wireless lan,” in *Proc. 3rd International Symposium on Communications, Control and Signal Processing ISCCSP 2008*, 12–14 March 2008, pp. 758–761.
  - [13] P. Godlewski, M. Maqbool, M. Coupechoux, and J.-M. Kélib, “Analytical evaluation of various frequency reuse schemes in cellular OFDMA networks,” in *ValueTools '08: Proceedings of the 3rd International Conference on Performance Evaluation Methodologies and Tools*. ICST, Brussels, Belgium, Belgium: ICST (Institute for Computer Sciences, Social-Informatics and Telecommunications Engineering), 2008, pp. 1–10.
  - [14] R. Y. Chang, Z. Tao, J. Zhang, and C. C. J. Kuo, “A graph approach to dynamic fractional frequency reuse (FFR) in multi-cell OFDMA networks,” in *Proc. IEEE International Conference on Communications ICC '09*, 14–18 June 2009, pp. 1–6.
  - [15] R. Srinivasan and et al., *IEEE 802.16m Evaluation Methodology Document (EMD), C802.16m-07-080r2*, IEEE 802.16 Broadband Wireless Access Working, Task Group m Std., June 2007.
  - [16] Y. Medjahdi, M. Terre, D. L. Ruyet, and D. Roviras, “Asynchronous OFDM/FBMC interference analysis in selective channels,” in *Proc. IEEE International Symposium on Personal, Indoor and Mobile Radio Communications (PIMRC '10)*, 2010.
  - [17] Y. Medjahdi, M. Terre, D. L. Ruyet, D. Roviras, and A. Dziri, “Performance analysis in the downlink of asynchronous OFDM/FBMC based multicellular networks,” 2010.
  - [18] European project ICT-211887 PHYDYAS, “Deliverable D6.2: Duplexing and multiple access techniques, software description,” <http://www.ict-phydyas.org>, Tech. Rep., December 2009.
  - [19] H. M. Salkin and K. Mathur, *Foundations of integer programming*. North-Holland, 1989.
  - [20] *IEEE Standard for Local and Metropolitan Area Networks Part 16: Air Interface for Fixed Broadband Wireless Access Systems*, IEEE Std. 802.16-2004 (Revision of 802.16-2001).

- [21] K. Wongthavarawat and A. Ganz, "Packet scheduling for QoS support in IEEE 802.16 broadband wireless access systems," *International Journal of Communication Systems*, vol. 2003, pp. 81–96, 2003.
- [22] C. Cicconetti, A. Erta, L. Lenzi, and E. Mingozzi, "Performance evaluation of the IEEE 802.16 MAC for QoS support," vol. 6, no. 1, pp. 26–38, Jan. 2007.
- [23] WiMAX Forum, "Mobile WiMAX - part I: A technical overview and performance evaluation," Aug 2006.
- [24] V. T. Raisinghani and S. Iyer, "Cross-layer feedback architecture for mobile device protocol stacks," *IEEE Commun. Mag.*, vol. 44, no. 1, pp. 85–92, Jan. 2006.
- [25] X. Wang and K. Kar, "Cross-layer rate optimization for proportional fairness in multi-hop wireless networks with random access," *IEEE J. Select. Areas Commun.*, vol. 24, no. 8, pp. 1548–1559, Aug. 2006.
- [26] W. Ge, J. Zhang, and S. Shen, "A cross-layer design approach to multicast in wireless networks," *IEEE Trans. Wireless Commun.*, vol. 6, no. 3, pp. 1063–1071, March 2007.
- [27] M. van der Schaar and D. S. Turaga, "Cross-layer packetization and retransmission strategies for delay-sensitive wireless multimedia transmission," *IEEE Trans. Multimedia*, vol. 9, no. 1, pp. 185–197, Jan. 2007.
- [28] J. Villalon, P. Cuenca, L. Orozco-Barbosa, Y. Seok, and T. Turletti, "Cross-layer architecture for adaptive video multicast streaming over multirate wireless LANs," *IEEE J. Select. Areas Commun.*, vol. 25, no. 4, pp. 699–711, May 2007.
- [29] L. Haratcherev, J. Taal, K. Langendoen, R. Lagendijk, and H. Sips, "Optimized video streaming over 802.11 by cross-layer signaling," *IEEE Commun. Mag.*, vol. 44, no. 1, pp. 115–121, Jan. 2006.
- [30] D. Triantafyllopoulou, N. Passas, A. Salkintzis, and A. Kaloxylos, "A heuristic cross-layer mechanism for real-time traffic over IEEE 802.16 networks," *Wiley's International Journal of Network Management*, vol. 17, no. 5, pp. 347–361, 2007, special issue on "Management Solutions for QoS Support over the Entire Audio-Visual Service Distribution Chain".
- [31] S. Khan, Y. Peng, E. Steinbach, M. Sgroi, and W. Kellerer, "Application-driven cross-layer optimization for video streaming over wireless networks," *IEEE Commun. Mag.*, vol. 44, no. 1, pp. 122–130, Jan. 2006.
- [32] H. Jiang and W. Zhuang, "Cross-layer resource allocation for integrated voice/data traffic in wireless cellular networks," *IEEE Trans. Wireless Commun.*, vol. 5, no. 2, pp. 457–468, Feb. 2006.

- [33] F. Yu, V. Krishnamurthy, and V. C. M. Leung, "Cross-layer optimal connection admission control for variable bit rate multimedia traffic in packet wireless CDMA networks," *IEEE Trans. Signal Processing*, vol. 54, no. 2, pp. 542–555, Feb. 2006.
- [34] Y. J. Zhang and K. B. Letaief, "Cross-layer adaptive resource management for wireless packet networks with OFDM signaling," *IEEE Trans. Wireless Commun.*, vol. 5, no. 11, pp. 3244–3254, November 2006.
- [35] C. Long, X. Guan, and B. Li, "Cross-layer congestion control, scheduling and power control design in multihop networks with random access," in *Proc. IEEE International Conference on Multimedia and Expo*, 9–12 July 2006, pp. 1125–1128.
- [36] IST-2001-32620 - MATRICE, "D1.3: Specification of the performance evaluation methodology and the target performance," Tech. Rep., December 2002.
- [37] *IEEE-802.16e-2006: IEEE Standard for Local and Metropolitan Area Networks Part 16: Air Interface for Fixed and Mobile Broadband Wireless Access Systems Amendment 2: Physical and Medium Access Control Layers for Combined Fixed and Mobile Operation in Licensed Bands and Corrigendum 1*, IEEE Std., 2006.